# Bactericidal activity of ZnO nanoparticles-anti TB drugs combination towards H37Rv strain and multidrug-resistant isolates of *Mycobacterium tuberculosis* via SufB splicing inhibition

Deepak Kumar Ojha[1], Ashwaria Mehra[1], Sunil Swick Rout[1], Sidhartha Giri[2] and Sasmita Nayak[1]*

[1]School of Biotechnology, Kalinga Institute of Industrial Technology Deemed to be University (KIIT-DU), Bhubaneswar, Odisha 751024, India

[2]National Reference Laboratory for Tuberculosis, ICMR-Regional Medical Research Centre (RMRC), Bhubaneswar, Odisha, 751023, India

*Corresponding Author: Dr. Sasmita Nayak, Email Id: sasmita.n@kiitbiotech.ac.in.

**Abstract**

Tuberculosis (TB) remains a significant global health threat, claiming millions of lives annually. Despite advancements in treatment, the emergence of drug-resistant strains has hindered effective TB control. The current management for TB is prolonged with severe side effects, leading to poor patient compliance. Metal-based nanoparticles are shown to manage drug-sensitive TB when combined with anti-TB drugs. However, mycobactericidal potential of nanoparticles towards drug-resistant TB is not confirmed yet. This work explores the bactericidal potential of Zinc Oxide Nanoparticles (ZnONPs, 40 nm) in managing both drug-sensitive and drug-resistant TB in combination with anti-TB drugs. It was found that ZnONPs inhibit generation of active SufB protein via splicing inhibition, an essential event for *Mycobacterium tuberculosis* (*Mtb*) survival. While TEM and UV-visible spectroscopy identified NPs~protein interaction, SEM visualised extensive membrane damage in H37Rv and multidrug-resistant (MDR) *Mtb* cells. Alamar blue assay and spread plate method detected minimum inhibitory concentration and minimum bactericidal concentration of ZnONPs towards H37Rv strain and MDR *Mtb* isolates. *In vitro* studies identified a combination with ZnONPs that reduced effective doses for anti-TB drugs towards H37Rv and MDR *Mtb* isolates.

A correlation to splicing inhibition was made by performing Alamar blue assay in SufB intein-less microbe, *Mycobacterium smegmatis*. A similar drug combination, attenuated the mycobacterial load, inflammation in the spleen & lungs, and protected against *Mtb* induced splenomegaly in infected mice. Thus, ZnONPs can be used as potent additive in anti-TB regimen to manage drug-susceptible and drug-resistant TB, addressing challenges such as prolonged therapy, drug toxicity and poor patient compliance.

**Keywords:** *Mycobacterium tuberculosis* H37Rv**;** SufB Intein; splicing regulation; ZnONPs; NPs/anti-TB drug combination; Drug-resistant TB

**Running title:** ZnONPs exhibit bactericidal activity towards MDR *Mtb*

**Number of Figures:** 8

## 1. Introduction

Tuberculosis (TB) is one of the leading causes of death worldwide, ranking among the top ten deadliest diseases globally, and is the single most lethal infectious agent, surpassing even HIV/AIDS [1,2]. However, efforts to combat TB are often impeded by several challenges, including absence of an effective vaccine, the complexities of treatment regimens, and the rapid emergence of drug-resistant *Mycobacterium tuberculosis* (*Mtb*) strains [3,4]. Moreover, prolonged therapy can lead to the phenomenon of cross-resistance, where bacteria become resistant to multiple drugs by exploiting shared mechanisms of action [5]. The standard treatment for drug-susceptible and drug-resistant TB spans approximately 6 months and over 18 months, respectively. The intricacy of these regimens, along with drug-induced side effects, often leads to poor patient compliance, worsening the current situation due to the emergence of new drug-resistant strains [6]. Hence, there is an urgency to develop next-generation strategies to mitigate the limitations and enhance the accessibility of TB management .

One promising approach to control TB could be targeting the intein splicing, which is a critical intracellular process that enables *Mycobacterium tuberculosis* (*Mtb*) survival and persistence by generating essential proteins [7,8]. Inteins are intervening polypeptides co-translated within the host precursor proteins and self-excised through protein splicing to generate active protein [9]. Given, that several human pathogens harbour inteins within vital proteins, and intein splicing is critical for their survival, the regulation of splicing can function as a promising target for developing anti-microbial drugs especially towards drug-resistant organisms. *Mtb* SufB, which is an Fe-S cluster assembly protein represents a notable example among mycobacterial proteins, for its significance in disease pathogenesis [10,11]. The SUF system as a whole is required for metalloprotein biogenesis and plays an important role in mycobacterial survival during iron limitation including oxidative and nitrosative stresses within infected macrophages [12,13].

In recent years, the synergistic integration of nanotechnology and medicine has emerged as a popular and diverse approach, particularly for the development of anti-microbial compounds. The convergence of these disciplines has demonstrated significant potential in addressing various challenges associated with bacterial infections [14–16]. Further, the interaction between nanoparticles and proteins holds significant importance in various areas of contemporary biomedical research, particularly in the fields of nanomedicine and nano diagnostics [17–21]. When nanoparticles interact with proteins, they form a protein corona, which alters the biological activity of the bound protein. This phenomenon has profound implications for understanding the behaviour of nanoparticles within biological environments and their potential applications in drug delivery, diagnostics, and therapeutics [22–29].

Thus, nanotechnology is gaining popularity as the cornerstone of modern research and therapeutics. This frequently involves metal-based NPs like ZnONPs that offer varied uses in emerging applications such as antimicrobial, anti-inflammatory, anti-tumour, and in wound

healing [30–35]. ZnONPs exhibit superior bioactivity, primarily due to their small size, and increased surface area to volume ratio [36]. ZnONPs are also preferred as efficient drug delivery vehicles for various diseases including cancer, because of their safety, stability, and low cost [36,37].

Previous research have shown the bacteriostatic effects of ZnONPs towards both drug-sensitive and extensively drug-resistant (XDR) *Mtb* strains at concentrations equal to or higher than 1 µg/ mL [38]. The same study has also determined 4 µg/mL as the inhibitory concentration of ZnONPs against the multidrug-resistant (MDR) strain of *Mtb*. Another work has reported the bactericidal role of ZnONPs - Se against *Mtb* BCG and H37Rv strains [39]. The antimicrobial mechanisms for ZnONPs effects are mostly attributed to a cumulative effect of cell membrane disruption, ROS production, release of toxic $Zn^{2+}$ ions, and toxicity induced by their photocatalytic action [40]. Although ZnONPs are known to exhibit potent antimicrobial and fungicidal activity towards different microbes [41], their bactericidal potential on drug-resistant *Mtb* strains are not shown till date. In a different context, inhibitory effects of divalent metal ions such as $Zn^{2+}$, and $Cu^{2+}$ on the splicing of various intein containing precursor proteins were explored extensively, but studies showing intein splicing attenuation in presence of metal-based NPs is missing till date [8,42–47].

Current study addresses the following questions: 1) Whether ZnONPs can regulate *Mycobacterium tuberculosis (Mtb)* SufB intein splicing and N-terminal cleavage reactions? 2) Since intein splicing generates a functional SufB protein that is critical for mycobacterial survival, whether ZnONPs mediated regulation of SufB splicing can affect the viability of whole cell *Mtb?* 3) Importantly, if, the viability of both drug-sensitive and drug-resistant strains of *Mtb* are influenced by ZnONPs? Next, 4) what is the minimum effective concentration of ZnONPs for the observed effect? 5) Whether ZnONPs combination can reduce the required dosage of existing anti-TB drugs to control both drug-sensitive and drug-resistant *Mtb*

102 infection? 6) Whether ZnONPs exhibit a bacteriostatic or bactericidal effect towards drug-
103 sensitive and drug-resistant *Mtb* strains*?* 7) Can ZnONPs protect against the effects of *Mtb*
104 infection in an animal model?
105 In this work, ZnONPs (40 nm) activity on the splicing and N-terminal cleavage reactions of
106 the *Mycobacterium tuberculosis* (*Mtb*) SufB precursor protein was examined. Initial
107 cytotoxicity evaluation via MTT assay indicated that ZnONPs are biocompatible towards
108 HEK293T cells (human embryonic kidney cell lines), up to a concentration of 50 µg/ml,
109 consequently rest of the experiments were performed within this limit. UV-Vis spectroscopy
110 confirmed ZnONPs ~ SufB interaction, further visualised by Transmission Electron
111 Microscopy (TEM), which identified protein "corona" formation around the ZnONPs.
112 Additional experiments like Dynamic Light Scattering (DLS), and zeta potential confirmed
113 ZnONPs-*Mtb* SufB interaction. Next, ZnONPs over varied concentration range (0.5 µg/ml-50
114 µg/ml) significantly inhibited the splicing and N-terminal cleavage reactions of *Mtb* SufB
115 precursor protein as shown by *in vitro* protein refolding assay. SDS-PAGE and Western blot
116 analyses visualized and confirmed the splicing and cleavage products. Further, Alamar blue
117 assay and spread plate method detected anti-mycobacterial activity of ZnONPs with a
118 minimum inhibitory concentration (MIC) / minimum bactericidal concentration (MBC) of 5
119 µg/ml/17 µg/ml and 14 µg/ml/23 µg/ml towards H37Rv strain (drug-sensitive) and multidrug-
120 resistant (MDR) *Mtb* isolates respectively. In a comparative study, we also observed a
121 reduction in the effective dose of anti- TB drugs INH/RIF and LFX/MXF in combination with
122 ZnONPs that could efficiently kill H37Rv strain and multidrug-resistant (MDR) *Mtb* isolates
123 respectively. The observed activity was correlated to splicing inhibition by performing Alamar
124 blue assay in SufB intein-less microbe *Mycobacterium smegmatis*. Scanning Electron
125 Microscopy (SEM) demonstrated mycobactericidal activity of ZnONPs towards both drug-
126 sensitive and drug-resistant *Mtb* (H37Rv) strains. Finally, infected mice model study revealed

127 that ZnONPs in combination with anti-TB drugs can effectively reduce mycobacterial load in
128 the lungs and spleen. The observed effects were noticed when ZnONPs was administered as a
129 solo therapy or in combination with a reduced dose of RIF compared to previously
130 recommended amount of RIF. Likewise, the same combination of ZnONPs - RIF, not only
131 attenuated the inflammation in lungs and spleen, but also provided resistance to splenomegaly
132 in the infected mice. Therefore, we suggest the use of ZnONPs as a promising adjunctive
133 therapy along with standard anti-TB drugs to combat both drug-sensitive and multidrug-
134 resistant *Mtb* infections, by inhibiting the splicing of an essential protein, *Mtb* SufB. This
135 approach may not only mitigate the toxicity associated with conventional and contemporary
136 anti-TB regimens but also potentially reduce the duration of therapy, thereby enhancing patient
137 compliance.

138 **2. Materials and Methods**

139 *2.1 ZnO nanoparticles*

140 ZnONPs (≥ 40 nm) were procured from Sigma Aldrich (Product #721077).

141 *2.2 MTT Assay* [48–50]

142 The cytotoxic effects of ZnONPs were evaluated using the MTT (3-[4,5-dimethylthiazol-2-yl]-
143 2,5-diphenyltetrazolium bromide) assay over a period of 72h. HEK239T cells ($10^4$ cells/well)
144 [Product # HEK239T (Human embryonic kidney cell line, ATCC (CRL-3216)] were seeded in
145 Dulbecco's Modified Eagle Medium (DMEM, Gibco, Invitrogen-2562497) in a 96-well plate
146 (200 µl per well) and allowed to adhere for 24 hours at 37°C in 5% $CO_2$ incubator.
147 Subsequently, varying concentrations of ZnONPs (5 µg/ml, 14 µg/ml, 17 µg/ml, 23 µg/ml
148 µg/ml, 26 µg/ml, 50 µg/ml, 100 µg/ml, 150 µg/ml) were added, followed by incubation at
149 37°C in 5% $CO_2$ incubator for 72 hours. HEK239T cells ($10^4$ cells/well) incubated in absence
150 of nanoparticles was considered as the control for 100% viable cell growth. DMEM culture

151 medium alone was used as blank control. 20 µl of MTT (EZcount™ MTT cell assay kit,
152 Himedia-CCK003) solution (5 mg $ml^{-1}$ in incomplete medium) was added to each well and
153 incubated for 3h to facilitate formation of purple formazan crystals under standard culture
154 conditions. Next, MTT solution was discarded, and the crystals were solubilized by gently
155 stirring on orbital shaker for 30 minutes. After solubilization, the absorbance (570 nm) of each
156 well was measured by using the ELISA plate reader (Bio Teck Epoch Microplate
157 Spectrophotometer). The percentage of cell viability was calculated using the following
158 formula.

159 $$\%\ of\ Cell\ viability = \frac{optical\ density\ (OD570) test\ sample - optical\ density\ (OD570) blank\ control}{OD570\ growth\ control - OD570\ blank\ control} \times 100$$

160 *2.3 UV Visible spectroscopy* [51–53]

161 Purified *Mtb* SufB precursor protein was refolded in presence of different concentrations of
162 ZnONPs (0.5 µg/ml, 26 µg/ml, and 50 µg/ml) as explained in section 2.7 for *in vitro* refolding
163 assay. Then, the treated samples were analyzed via UV-Visible spectroscopy (UV-1800
164 Shimadzu) over the visible region of the spectrum (200-800 nm). To account for potential
165 buffer-nanoparticle interactions, control samples included refolding buffer (20 mM sodium
166 phosphate, 0.5 M NaCl, 0.5 M arginine, and 8 M urea) alone and the buffer with 50 µg/ml of
167 nanoparticles incubated under the same conditions. The nanoparticle-treated buffer served as a
168 blank for baseline correction. The absorbance results were analyzed by plotting absorbance
169 versus wavelength using OriginPro 8.5 (Version 8.5, OriginLab Corporation, Northampton,
170 MA, U.S.A.).

171 *2.4 Quantification of NPs-bound proteins via Bradford assay* [54–56]

172 The quantification of adsorbed protein was conducted using the Bradford assay. *Mtb* SufB
173 precursor protein was renatured *in vitro* both in presence and absence various concentrations
174 of ZnONPs (0.5 µg/ml, 26 µg/ml, and 50 µg/ml) for 4 hours, as mentioned in section 2.7. Next,

175 the protein-NPs mixture was centrifuged at 13,000 rpm for 30 minutes, at 4°C, to separate the
176 protein-bound nanoparticles. Then, the pellet containing the protein ~ NPs was resuspended in
177 100 µl of 1×PBS and analysed using Bradford reagent to quantify the amount of adsorbed
178 proteins. Control samples included nanoparticles in 1×PBS and test proteins resuspended in
179 1×PBS.

180 *2.5 TEM Analysis* [57,58]

181 *Mtb* SufB precursor protein-ZnONPs interaction was analysed by Transmission Electron
182 Microscope (Jeol JEM-1400) for visualising protein corona formation. *Mtb* SufB precursor
183 protein was overexpressed, purified and refolded with 50 µg/ml of ZnONPs as mentioned in
184 section 2.7. The protein-ZnONPs complex was collected via centrifugation (13,000 rpm for 30
185 minutes) at $4^0$C, washed twice with phosphate buffer saline (1×PBS) and the supernatant was
186 discarded. Then the pellet (protein-ZnONPs complex) was resuspended and fixed with 100 µl
187 of 2.5% glutaraldehyde in 1×PBS for 1 hr. Finally, 5 µl of solution (ZnONP-complex) was
188 placed onto the carbon-coated copper grid and imaged under TEM with an acceleration voltage
189 of 120 Kv.

190 *2.6 Purification of overexpressed proteins*

191 The details of the plasmids used in this study are provided elsewhere [7]. The *Mtb* SufB wild
192 type precursor, and *Mtb* SufB splicing inactive double mutant (C1A/N359A) (splicing negative
193 control), all carrying an N-terminal 6X His tag, were overexpressed in BL21 (DE3) *E. coli* cells
194 via IPTG (500 µM, sigma 367-93-1) induction. The cells were resuspended in lysis buffer
195 (20mM sodium phosphate, 0.5M NaCl, pH 7.4) and lysed using a tip sonicator (Sonics vibra
196 cell VCX-130) [59]. The cell lysate was centrifuged at 16,500xg for 20 minutes at 4°C and the
197 supernatant was discarded. The collected IB materials were washed thrice via centrifugation in
198 lysis buffer, solubilized in 8 M urea (Merck, 1084870500) buffer (lysis buffer, 8M urea, 10

199 mM imidazole (MP–biochemicals-288-32-4), and centrifuged at 16,500xg for 20 minutes at
200 4°C to collect the supernatant. The solubilized proteins were purified using a Ni-NTA affinity
201 column (Ni-NTA His trap, HP GE healthcare life sciences- 17524802) [60–64]. Before sample
202 application, the columns were equilibrated with binding buffer (20 mM sodium phosphate, 0.5
203 M NaCl, 8 M urea, 10 mM imidazole), and after loading the samples, the columns were washed
204 several times (15 column volumes) with the wash buffer (20 mM sodium phosphate, 0.5M
205 NaCl, 8M urea, 40 mM imidazole). Finally, the test proteins were eluted in elution buffer
206 (20mM sodium phosphate, 0.5M NaCl, 500 mM imidazole, 8 M Urea, pH 7.4) and quantified
207 using Bradford's assay.

208 *2.7 In vitro protein refolding and splicing analysis via SDS gradient PAGE*

209 Denatured test proteins (2.5 μM) in 8M urea buffer were renatured in a refolding buffer
210 containing 20 mM sodium phosphate, 0.5 M NaCl, 0.5 M L-Arginine (A5006 Sigma Aldrich),
211 and 2 mM TCEP-HCl (Sigma-51805-45-9). Protein refolding was performed for 4 hours at
212 25ºC [59–64] in the presence and absence of ZnO nanoparticles (ZnONPs) over a varied
213 concentration range (0.5 μg/ml to 50 μg/ml). For the 0-hour sample, protein sample was
214 collected before initiation of the refolding, followed by immediate addition of the loading dye
215 (0.1% bromophenol blue, 50% glycerol, β-mercaptoethanol, 10% SDS, tris, pH 6.8) and rapid
216 freezing at -20ºC. After 4h of protein renaturation, rest of the samples were collected, loading
217 dye was added, samples were boiled at 95ºC for 5 minutes. Then protein products were resolved
218 through 5~10% gradient SDS-PAGE gel. The protein bands were visualized by staining with
219 Coomassie brilliant blue R-250 (Catalogue no #112553, Sigma-Aldrich), and densitometric
220 analysis was performed using the GelQuant.Net biochemical solutions software. The splicing
221 and cleavage efficiencies were calculated as the percentage ratio of the total splicing product
222 (LE and I) over the total proteins (LE+I+P) and the total N-terminal cleavage product (NE+NC)
223 over the total proteins (NE+NC+P), respectively. 0-hour splicing and cleavage product values

224 were subtracted from respective sample values for baseline corrections. The results were
225 analysed using one-way ANOVA and plotted using GraphPad Prism version 5.01 for
226 Windows, GraphPad Software, San Diego, CA, U.S.A., www.graphpad.com.

227 *2.8 Western blot analysis* [8]

228 For Western blot analysis, an anti-His antibody was utilized to confirm the presence of splicing
229 and N-terminal cleavage products. The test proteins were transferred from the 5-10% SDS-
230 PAGE to the PVDF membrane (Millipore, IPVH 00010) at a voltage of 10V, overnight at 4ºC.
231 Subsequently, the blot was blocked with 5% skim milk and incubated overnight at 4ºC. Then,
232 the membrane was washed once with 1× TBST (Tris-buffered saline with Tween-20) followed
233 by incubation with a primary anti-His antibody (abgenex-32-6116) at 1:5000 dilution
234 overnight at 4ºC. In the next step, the membrane was washed thrice for 5 minutes, with 1×TBST
235 and incubated with a secondary antibody (anti-mouse, abgenex 11-301) at a dilution of 1:6000,
236 for 6 hours at 25ºC. To enhance detection of the N-extein band, a higher dilution of the primary
237 antibody (1:2500) and secondary antibody (1:4000) were used. Finally, the blots were washed
238 with 1× TBST and developed using Enhanced Chemiluminescence Substrate (ECL) (abcam,
239 ab65628) to visualize the protein bands and images were captured using in-house
240 ImageQuant™ LAS 500 facility (GE Healthcare).

241 *2.9 Anti-mycobacterial study*

242 *2.9.1 Preparation of Mtb cells* [65]

243 Different mycobacterial cells [Drug sensitive H37Rv (ATCC-27294), H37Ra (ATCC-25177),
244 *M.sm* (ATCC-19420) and clinically isolated MDR *Mtb* isolates obtained from National
245 Reference Laboratory (NRL), ICMR-Regional Medical Research Centre (RMRC-ICMR),
246 Bhubaneswar, India] were grown in Middlebrook 7H9 broth (Merck-M0178) supplemented
247 with Middlebrook oleic acid, albumin, dextrose, and catalase (OADC) (Himedia-FD018). CFU

248 calculations were made by matching the turbidity of inoculum with McFarland standard
249 (Himedia- R092) against a black background. $10^6$ CFU of mycobacterial cells were used for
250 subsequent experiments.

251 *2.9.2 Alamar blue assay* [66–68]

252 $10^6$ CFU of mycobacterial cells were incubated with different concentrations of ZnONPs (0.5
253 ug/ml to 50 ug/ml) in 96-well microtiter plates. For a comparative study, cells were also
254 incubated with anti- TB drugs Isoniazid (INH), Rifampicin (RIF), Moxifloxacin (MXF), and
255 Levofloxacin (LFX) to evaluate their activity towards H37Rv strain and multidrug-resistant
256 (MDR) *Mtb* isolates. The plates were sealed and incubated at 37ºC for 14 days. Later, 10%
257 (v/v) solution of Alamar Blue reagent (SRL-42650) was added to each well and the plates were
258 incubated at 37ºC for 24 hours. The anti-mycobacterial efficacy of each compound was
259 evaluated based on the observed colour change. Live cells were identified by transition of
260 colour from blue to pink whereas dead cells remained blue. The minimum inhibitory
261 concentration (MIC) for ZnONPs and anti-TB drugs were determined as the lowest
262 concentration at which cell viability was inhibited partially, resulting in a purple colour.

263 *2.9.3 Spread plate method to determine Minimum Bactericidal Concentration (MBC)* [69]

264 Mycobacterial cells at $10^6$ CFU were incubated with different concentrations of ZnONPs (0.5
265 μg/ml to 50 μg/ml) for 14 days in 96 well microtiter plates. Then, sample (1:1000 dilution)
266 from each well was evenly spread onto respective 7H10 agar (Himedia- M199) plate using a
267 sterile spreader. The plates were incubated at 37ºC for 21days to grow mycobacterial colonies.
268 Subsequently, colonies were counted by colony counting method and MBC was determined as
269 the lowest concentration of the test compounds at which no colony growth was visualised on
270 the respective agar plates. Controls plates included mycobacterial cells without NPs treatment.
271
272

273 *2.9.4 Scanning Electron Microscopic (SEM) analysis* [70]

274 $10^6$ CFU of mycobacterial cells were incubated with different concentrations (0.5 μg/ml,17
275 ug/ml, 26 μg/ml, and 50 μg/ml) of ZnONPs in 7H9 broth medium for 7 days. Then, cells were
276 harvested, fixed with 2.5% glutaraldehyde, and dehydrated with a series of ethanol treatment
277 (30%, 60%, 70%, 80%, and 90%). Finally, cells were treated with 100% ethanol for 30 min.
278 Then gold-palladium particles were sputtered over the mycobacterial cells by an automated
279 sputtering machine and visualized via SEM (Hitachi, S-3400N), CIF, OUAT, Bhubaneswar.

280 *2.9.5 Animal experiments* [66]

281 Female BALB/c mice, aged 6 to 8 weeks and weighing each 25 ± 2 g, were used for the study.
282 Mice were randomly divided into three groups, each consisting of 6 to 8 mice. The animals
283 were injected intravenously with 5 x $10^6$ colony-forming units (CFU) of *Mycobacterium*
284 *tuberculosis* (strain H37Ra) over a period of 4 days. Subsequently, ZnONPs were orally
285 administered to the infected mice at different concentrations (26 and 50 μg/ml) for 7 days post-
286 infection. Rifampicin alone, given orally at a dose of 15 mg/kg to the infected mice was used
287 as a positive control, while mice who were given oral 1×PBS served as the negative control.
288 After 18 days of infection, the mice were euthanized under 5% inhaled isoflurane anaesthesia
289 (Sigma-792632), followed by cervical dislocation. Then, their lungs and spleen were isolated
290 and processed for histopathological examination and estimation of mycobacterial load via CFU
291 analysis. A portion of the lung was fixed in 4% paraformaldehyde for 48 hours and then
292 embedded in paraffin to prepare sections for haematoxylin and eosin staining. Next, lung and
293 spleen homogenates in 1×PBS were plated onto Middlebrook 7H11 agar, supplemented with
294 OADC (Himedia-FD018) and BBL MGIT PANTA antibiotics (Catalogue #245114, BD,
295 United States), to quantify the bacterial burden. Culture plates were incubated for 3 to 4 weeks
296 at 37°C, followed by calculation of CFU by colony counting methods.

297

298 *2.10 Statistical analysis*

299 For each method, numerical data from three to six independent sets of experiments were
300 analysed using GraphPad Prism 6.0 (La Jolla, CA, United States) and are presented as mean ±
301 1 standard deviation or standard error of the mean. Statistical significance between different
302 groups was assessed using one-way ANOVA, with significance denoted by $p < 0.05$. Specific
303 p-values of <0.05, <0.01, <0.001, and <0.0001 were indicated as *, **, ***, and ****,
304 respectively.

305 **3. Results and discussions**

306 *3.1 ZnONPs interact with Mtb SufB precursor protein*

307 Previous studies have reported interaction of nanoparticles with biological molecules such as
308 proteins and DNA [71]. Before examining the role of ZnONPs on the splicing activity, we
309 evaluated possible interaction between ZnONPs and *Mtb* SufB precursor protein. Through a
310 combination of analytical techniques such as UV-visible spectroscopy, Bradford analysis, and
311 transmission electron microscopy (TEM), we have evaluated ZnONPs~protein binding activity
312 (Figure 1).

313 Initially, cytotoxicity of the ZnONPs was assessed via MTT assay using human embryonic
314 kidney cell line, HEK239T cells, since potentially harmful NPs are mostly excreted by kidney
315 through urine [72–74]. It was demonstrated that up to a concentration of 50 µg/ml, ZnONPs
316 exhibited no cytotoxicity against HEK239T cells (Figure S1, Supplementary Information).
317 This is further supported by a prior research which has shown similar results [75]. Consequently,
318 we decided to explore SufB interaction with various ZnONPs concentrations up to this limit
319 (0.5, 26, and 50 µg/ml). UV–Visible spectra for both the *Mtb* SufB precursor protein and
320 ZnONPs-SufB complexes were recorded by scanning over the visible range (200 to 800 nm),
321 as depicted in Figure 1A. Buffer alone and buffer along with nanoparticles (50 µg/ml) were
322 used for baseline correction and as the reference blank respectively. An observable broadening

323 and blue shift were differentiated in the absorbance spectra of the *Mtb* SufB protein following
324 interaction with increasing concentrations of ZnONPs, when compared to the spectra of protein
325 solubilised in buffer alone. This observation suggests the binding of ZnONPs with the *Mtb*
326 SufB precursor protein over test concentration range.
327 To further validate such interaction, we utilized Bradford assay, where *Mtb* SufB precursor
328 protein was refolded along with varying concentrations of ZnONPs (0.5, 26, and 50 µg/ml),
329 causing adsorption of proteins onto the NPs surface. After isolating ZnONPs-protein
330 complexes, quantification of bound proteins was done using Bradford assay. As illustrated in
331 Figure 1B, an increase in nanoparticle concentration correlated with a proportional increase in
332 the bound proteins. This result further supported the interaction between ZnONPs and *Mtb*
333 SufB protein.

334 The formation of a protein corona on NPs surfaces was investigated through TEM analysis, as
335 shown in Fig 1C. While standalone ZnONPs exhibited discrete distribution [1C(i)], NPs (50
336 µg/ml)-treated protein sample displayed a distinct feature. A thin, transparent layer encasing
337 the NPs was evident in the treated sample (yellow arrows) as seen in the Figures 1C(ii and iii).
338 This is indicative of the protein corona formed on the surface of the ZnONPs upon interaction
339 with the *Mtb* SufB protein [76].

340 DLS measurements demonstrated a significant increase in hydrodynamic diameter following
341 interaction of ZnONPs (26 µg/ml and 50 µg/ml) with *Mtb* SufB compared to controls (Buffer;
342 Buffer with *Mtb* SufB; Buffer with ZnONPs) (Figure S2A, Table S1, Supplementary
343 Information)[77]. Concomitant zeta potential analysis revealed a charge inversion from +5.1 mV
344 (bare ZnONPs) to -4 mV for the ZnONPs-SufB complex (Figure S2B, Table S1,
345 Supplementary Information)[77,78]. This transition from net positive to net negative surface
346 charge suggests a protein-nanoparticle binding event. Therefore, the observed changes in both

hydrodynamic size and surface charge distribution shows evidence for ZnONPs-SufB interaction.

The comprehensive assessment involving UV-visible spectroscopy, Bradford analysis, DLS, zeta potential analysis and TEM, successfully indicated the binding activity and protein corona formation following ZnONPs interaction with *Mtb* SufB.

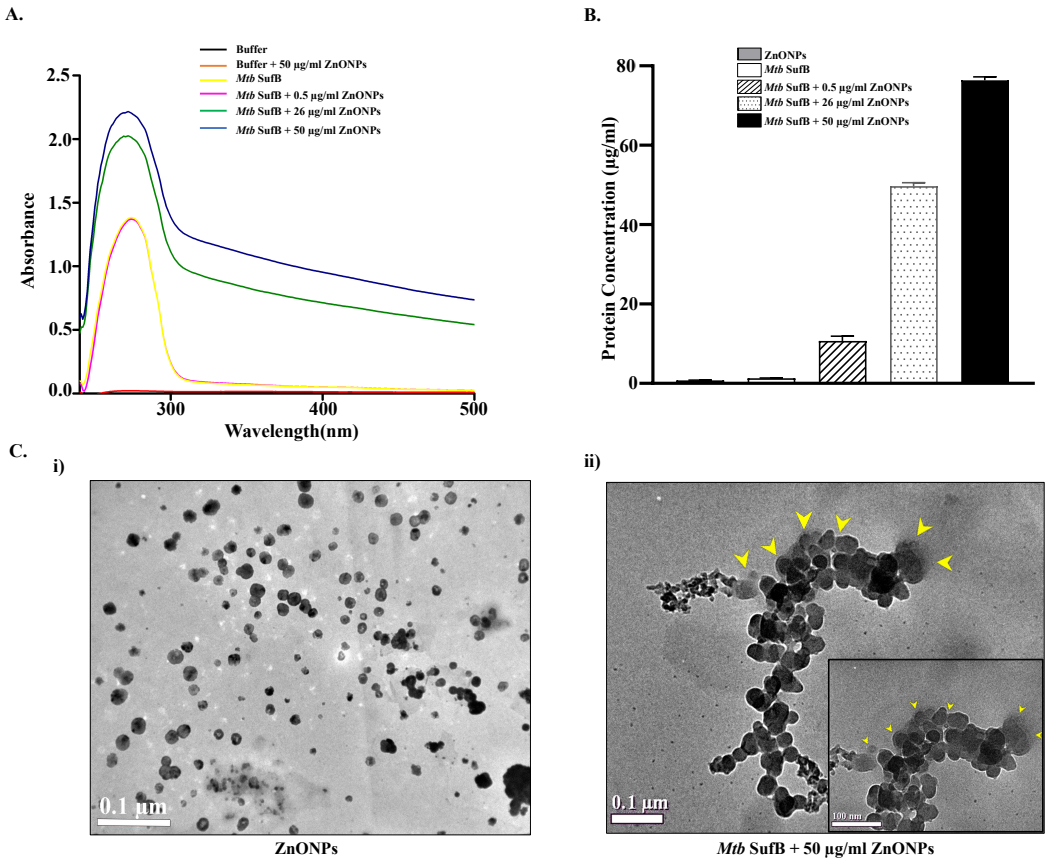


**Figure 1. Evaluation of ZnONPs interaction with *Mtb* SufB. A)** UV–Visible spectroscopy: *Mtb* SufB precursor protein was treated with ZnONPs (0.5 µg/ml, 26 µg/ml, 50 µg/ml), and sample absorbance was measured by scanning over 200–500 nm wavelength. **B)** Bradford Assay: Denatured test proteins were renatured *in vitro* in the presence of varied ZnONPs concentration for a period of 4 hrs at $25^0$C. Then, test samples were processed, and the concentration of adsorbed protein was determined using Bradford reagent. **C)** TEM Analysis: Images showing. (i) discrete ZnONPs and (ii) protein corona formation on the surface of ZnONPs aggregates after interaction with *Mtb* SufB (yellow arrows). The inset focuses on the protein shell around the ZnONPs.

375 *3.2 ZnONPs inhibit generation of functional SufB protein*

376 The SUF system provides an unique pathway for [Fe-S] cluster biosynthesis and *Mtb* survival
377 during intracellular stress like iron deprivation [79]. In such environments, the functionality of
378 the SUF complex relies exclusively on the splicing of *Mtb* SufB precursor to generate active
379 SufB protein [13]. Hence, splicing regulation under such physiological stress can lead to potential
380 anti-TB drug development strategies by influencing mycobacterial cell viability. Although
381 metals are known inhibitors of intein splicing [42,45,46], NPs mediated splicing inhibition has not
382 been reported yet. Further, higher reactivity of nanoparticles in a biological system has
383 prompted us to evaluate ZnONPs and *Mtb* SufB interactions with possible effects on SufB
384 precursor splicing.

385 *In vitro* splicing assay was conducted both in the presence and absence of ZnONPs, as detailed
386 in the methods section. Since, MTT assay demonstrated that HEK239T cells (human
387 embryonic kidney cell lines) were tolerant to ZnONPs up to a concentration of 50 µg/ml (Figure
388 S1, Supplementary Information), splicing efficiency was evaluated using NPs concentrations
389 up to this limit. Figure 2A illustrates different structural domains of *Mtb* SufB precursor
390 protein; N-extein (29.9 kDa), Intein (40.2 kDa), and C-extein (25.8 kDa). The details of *Mtb*
391 SufB splicing and N- terminal cleavage reactions are published elsewhere [7]. SufB precursor
392 undergoes splicing reactions to generate ligated exteins (LE), and intein (I), whereas N-
393 terminal cleavage reactions yield N-terminal cleavage product (NC, 65.2 kDa), and N-extein
394 (NE) (Figure 2A). Figures 2B(i) and 2B(ii) depict the concentration-dependent inhibition of
395 these reactions by ZnONPs, providing crucial insights into their biological role.

396 The samples were analyzed through gradient SDS-PAGE, and the bands were quantified using
397 the GelQuant.NET software. Our findings indicated a substantial inhibition of *Mtb* SufB
398 precursor splicing ($p<0.0001$) over all the test concentration range, with discernible effects
399 commencing at a ZnONPs concentration of 0.5 µg/ml. Remarkably, a complete inhibition of

splicing was observed at a concentration of 47 µg/ml [Figures 2B(ii) and C(i)]. These findings suggest that ZnONPs exert a dose-dependent inhibition of splicing in *Mtb* SufB precursor protein which could lead to critical consequences such as loss of functionality of this protein in a cellular environment.

Similarly, the N-terminal cleavage reaction of *Mtb* SufB precursor was notably inhibited ($p<0.0001$) in the presence of ZnONPs. A reduction in the cleavage activity was observed at the minimal tested concentration of 0.5 µg/ml, culminating in a complete inhibition at a concentration of 26 µg/ml [Figures 2B(i) and C(ii)]. Thus, ZnONPs exert a potent inhibitory effect on the *Mtb* SufB splicing and N-terminal cleavage reactions, underscoring their potential interference with SufB-associated cellular processes. These findings also highlight the significant biological implications of ZnONPs on *Mtb* survival within host cells. To substantiate these findings, we performed western blot analysis to validate identity of protein products (Figure S3, Supplementary Information), which further confirmed the inhibitory role of ZnONPs on the splicing and N-terminal cleavage reactions of SufB. Additional intermediate concentrations of ZnONPs were used to check the robustness of such effects on the splicing and cleavage activity of the precursor protein (Figure S4, Supplementary Information).

Current research presents evidence that ZnONPs interact with the *Mtb* SufB precursor protein, leading to a concentration-dependent inhibition of both splicing and N-terminal cleavage reactions. These findings also emphasize on the notable impact ZnONPs could have on the essential cellular processes linked to *Mtb* SufB protein, and their potential implications in biological systems. Specifically, it calls for further exploration into the influence of ZnONPs on SufB splicing, correlating this process to the growth and viability of *Mtb.*

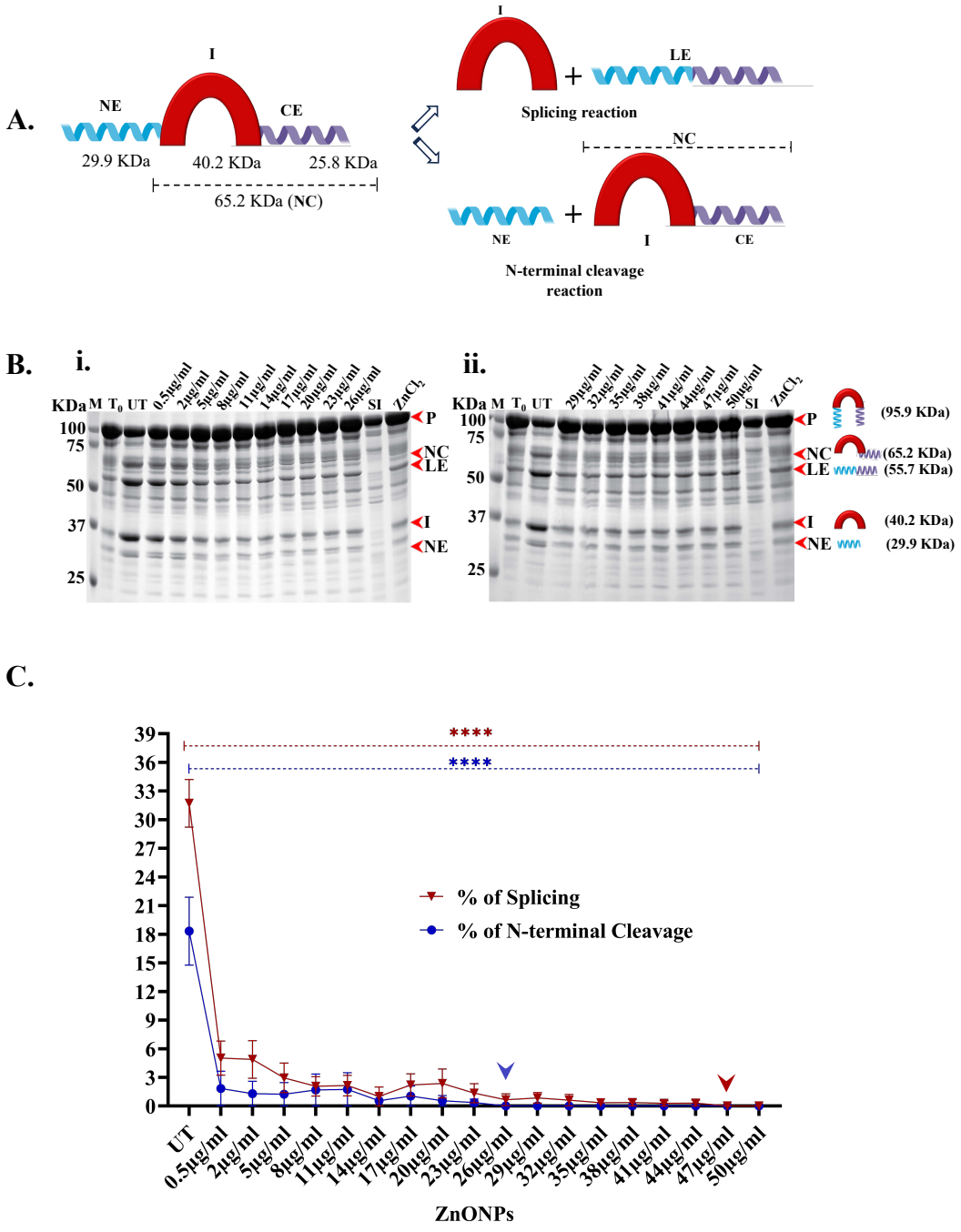


**Figure 2. Effect of ZnONPs on *Mtb* SufB precursor splicing and N-terminal cleavage reactions. (A)** Schematic diagram representing different structural domains of *Mtb* SufB precursor protein and splicing & N-terminal cleavage reactions of the precursor protein generating different protein products. **(B)** Products from *in vitro* protein refolding experiment were resolved through 5–10% gradient SDS-PAGE. ($T_0$): splicing and cleavage reactions at 0 h, (UT): untreated protein sample; and Lanes 4- 13 show protein products induced by varied concentrations ZnONPs: (i) (0.5 µg/ml -26 µg/ml)

450 (ii) (29 µg/ml to 50 µg/ml), Lane 14 (SI): Splicing inactive SufB double mutant (Cys1Ala/Asn359Ala)
451 is used as a negative control for splicing, Lane 15: $ZnCl_2$ (2 mM) was used as a positive control, since
452 it is a known inhibitor of *Mtb* SufB splicing reactions [8]. **(C)** Line plots showing the quantitative results
453 of splicing and N-terminal cleavage reaction inhibition. Values were extracted from Figure 2(B) and
454 plotted after densitometric analyses using GelQuant.Net biochemical solutions. 0h splicing, and
455 cleavage values were subtracted from each sample as baseline correction. The red arrow and blue arrow
456 denote complete inhibition of SufB splicing and N-terminal cleavage reactions by ZnONPs at
457 concentrations of 47 µg/ml and 26 µg/ml, respectively. Error bars represent (±1) SEM from (n=3) three
458 independent sets of experiments ($p<0.0001$). P: precursor, NC: N-terminal cleavage product, LE: ligated
459 extein, I: intein, and NE: N-extein.
460
461 *3.3 ZnONPs inhibit the growth and viability of Mycobacterial cells*
462 Since ZnONPs were shown to interact with the SufB precursor protein, and caused inhibition
463 of protein splicing, it was imperative that this may retard the growth and viability of *Mtb* by
464 blocking the generation of an essential protein SufB. Both H37Rv cells and MDR *Mtb* isolates,
465 were cultured in a nutrient medium along with various concentrations (0.5 µg/ml~50 µg/ml) of
466 ZnONPs, as discussed in the methods section. The test concentration range for the ZnONPs
467 were chosen based on their activity range as outlined in Figures 2B and 2C. Further, up to a
468 concentration of 50 µg/ml, ZnONPs exhibited no cytotoxicity against HEK239T cells (Figure
469 S1, Supplementary Information). Besides, ZnONPs at a concentration of ≥50 µg/ml was also
470 found to be toxic for human cells, elucidated by earlier research [80].
471 We performed Alamar blue assay, a well-established metric for cell viability, which yielded
472 data on the inhibitory roles of ZnONPs on the growth and survival of H37Rv and MDR *Mtb*
473 cells. The Alamar blue dye, initially blue, undergoes reduction in viable cells, resulting in a
474 colour change to pink, whereas persistence of the blue colour indicates lack of viable cells [81].
475 ZnONPs at 0.5 µg/ml and 2 µg/ml did not have any effect H37Rv cells. 5 µg/ml was identified
476 as the minimum inhibitory concentration (MIC) for ZnONPs at which H37Rv cells turned
477 purple due to partial loss of cell viability (Figure 3A). A complete loss of cell viability, and
478 retention of blue colour was noted at a concentration of 17 µg/ml of ZnONPs.

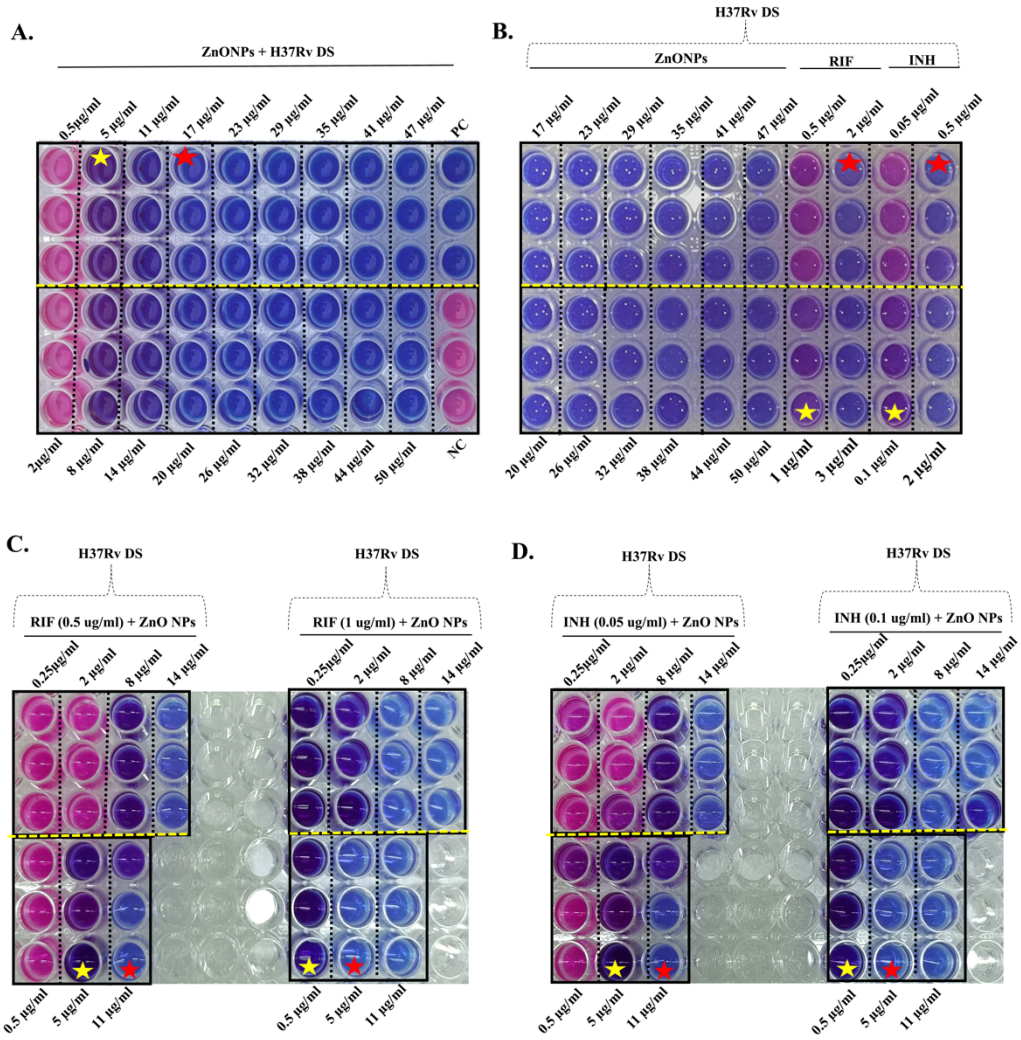


**Figure 3. Alamar blue assay to determine the minimum inhibitory concentrations (MIC) of ZnONPs towards H37Rv *Mtb* cells. (A)** Mycobacterial cells were incubated in a 96 well plate, in presence of varied concentrations (0.5 to 50 µg/ml) of NPs for 14 days, followed by addition of Alamar Blue reagent. Further incubation at 37ºC for 24 hours, led to colour change in the wells. MIC of ZnONPs was identified as 5 µg/ml where transition of blue to purple colour occurred suggesting partial loss of cell viability among the cells. Persistence of blue colour correlating to complete loss of viable cell population was seen at 17 µg/ml of ZnONPs. Pink cells refer to healthy viable cells resisting inhibitory effect of ZnONPs. **(B)** Comparison of the activity of first line anti-TB drugs; INH & RIF and varied concentration of ZnONPs. All the cells were rendered non-viable (blue) at a concentration of 17 µg/ml for the NPs, 2 µg/ml for RIF, 0.5 µg/ml for INH, and at respective higher concentrations. The MIC for RIF & INH as shown in this study coincided with the known values of 1 and 0.1 µg/ml respectively [82]. Synergistic activity of ZnONPs and anti-TB drugs; **(C)** RIF & **(D)** INH. $10^6$ CFU of bacterial cells were grown in presence of varied concentrations of ZnONPs and Drugs. A combination

508 of RIF (0.5 μg/ml)+ ZnONPs (11 μg/ml) & RIF (1 μg/ml)+ ZnONPs (5 μg/ml) successfully yielded
509 non-viable cells (blue). Likewise, INH (0.05μg/ml) + ZnONPs (11 μg/ml) & INH (0.1 μg/ml) +
510 ZnONPs (5 μg/ml) combinations resulted in non-proliferating cells (blue). Red stars- complete loss of
511 viability & Yellow stars- partial loss of viable cells (purple) at a lower concentration of NPs. DS: Drug
512 sensitive H37Rv *Mtb*, RIF: Rifampicin, INH: Isoniazid.
513

514 Next, a comparative study was conducted to assess the efficacy of ZnONPs in tandem with
515 first-line anti-TB drugs such as Rifampicin (RIF) and Isoniazid (INH) for which the Minimum
516 Inhibitory Concentrations (MICs) and Minimum bactericidal Concentrations (MBC) are well-
517 documented [82,83]. RIF and INH, at known MICs of 1 μg/ml and 0.1 μg/ml respectively, resulted
518 in partial loss of mycobacterial cell viability (purple colour) in the respective wells. There
519 was a complete loss of viable cell population (blue colour) at 2 μg/ml of RIF, and 0.5 μg/ml of
520 INH, comparable to the activity of ZnONPs at 17 μg/ml (Figure 3B). All the cells were
521 rendered non-viable at concentrations higher than these values.
522 Figures 3C and 3D depict the synergistic activity of ZnONPs and first line anti-TB drugs; RIF
523 & INH. A combination of RIF (0.5 μg/ml) + ZnONPs (11 μg/ml) & RIF (1 μg/ml) + ZnONPs
524 (5 μg/ml) successfully yielded non-viable cells (blue). Likewise, INH (0.05 μg/ml) + ZnONPs
525 (11 μg/ml) & INH (0.1 μg/ml) + ZnONPs (5 μg/ml) combinations resulted in non-proliferating
526 cells (blue). Thus, both RIF and INH at their respective MIC and half reduced MIC values
527 could completely abolish mycobacterial cell viability when added together with ZnONPs.
528 These results emphasize on the diminution in effective concentration for the conventional anti-
529 TB drugs (INH & RIF) in a combination with ZnONPs.
530 MIC values of ZnONPs towards multidrug-resistant (MDR) *Mtb* isolates were found to be
531 higher at 14 μg/ml (Figure 4A). The MBC values for the ZnONPs [17 μg/ml for drug-sensitive
532 H37Rv and 23 μg/ml for multidrug-resistant (MDR) *Mtb* isolates] were further confirmed
533 through agar spread plate method as shown in Supplementary Information (Figure S5,

534 Supplementary Information). Although MDR cells were rendered nonviable at 20 μg/ml of
535 ZnONPs (Figure 4A), based on the data obtained from agar spread plate method (Figure S5,
536 Supplementary Information), for the remaining experiments 23 μg/ml was considered as the
537 MBC for ZnONPs towards MDR *Mtb* cells.
538 In the case of MDR isolates, the anti-TB drugs Moxifloxacin (MXF) and Levofloxacin (LFX),
539 with known MICs of 0.0625 μg/ml and 0.125 μg/ml respectively[84,85], were compared with the
540 activity of the ZnONPs (Figure 4B). There was a complete loss of viable cell population (blue
541 colour) at LFX (0.25 μg/ml) / MXF (0.125 μg/ml) and their activity was comparable to the
542 effect of ZnONPs at 23 μg/ml (MBC) (Figure 4B). All the cells were rendered non-viable (blue)
543 at concentrations higher than these values for the test compounds. Thus, the antimycobacterial
544 activity of ZnONPs towards MDR *Mtb* isolates was comparable to that of anti-TB drugs MXF
545 and LFX at their respective MIC and higher values. This underscores the potential of ZnONPs
546 as a potent alternative for managing *Mtb* infections
547 Next, the synergistic activity of ZnONPs along with LFX and MXF was evaluated towards
548 MDR *Mtb* isolates (Figures 4C and 4D). A combination of LFX (0.0625 μg/ml)+ ZnONPs (17
549 μg/ml) and LFX (0.125 μg/ml)+ ZnONPs (11 μg/ml) resulted in non-viable cells (blue). A
550 similar observation was made for, MXF (0.031 μg/ml) + ZnONPs (17 μg/ml) and MXF (0.0625
551 μg/ml)+ ZnONPs (11 μg/ml) combinations towards the viability of MDR cells.
552 Thus, both LXF and MXF at their respective MIC and half reduced MIC values could
553 completely abolish mycobacterial cell viability when added together with ZnONPs. In toto,
554 these results suggest that ZnONPs exhibit anti-mycobacterial properties against both H37Rv
555 and MDR *Mtb* cells, indicating their potential utility as a supportive therapy in the fight against
556 TB.
557 On the whole, from the results of *in vitro* splicing and Alamar blue assays, ZnONPs-mediated
558 inhibition of mycobacterial growth could be attributed to splicing attenuation induced by

559 interactions between ZnONPs and *Mtb* SufB precursor protein. By targeting essential proteins
560 like the splicing of SufB, ZnONPs are likely to disrupt vital cellular processes in the
561 mycobacteria, leading to growth inhibition and loss of cell viability. To further correlate these
562 events, Alamar blue assay was performed to examine the effect of ZnONPs (0.5 ug/ml to 50
563 ug/ml) on the growth and viability of *Mycobacterium smegmatis* (*M. sm*), in which SufB
564 polypeptide chain lacks an intein sequence (Figure S6, Supplementary Information) [86]. Live
565 viable cells (pink) (Figure S6, Supplementary Information), indicated no effect of ZnONPs (0.5
566 µg/ml to 50 µg/ml) on *M. sm* viability, possibly due to lack of regulatory influence on SufB
567 splicing and cleavage reactions. This provided further evidence to support loss of *Mtb* cell
568 viability (alamar blue assay) as a result of ZnONPs mediated inhibition of *Mtb* SufB splicing
569 and cleavage reactions, although additional mechanisms such as NPs-mediated membrane
570 damage cannot be ruled out.
571 Furthermore, our investigation into combinatorial therapy, integrating lower effective
572 concentrations of known anti-TB drugs alongside ZnONPs, revealed a notable inhibitory effect
573 on the growth and viability of *Mycobacterium tuberculosis* (*Mtb*) cells. Particularly noteworthy
574 was the complete loss of cell viability observed at concentrations half of the MIC values for
575 the individual drugs along with a reduced effective concentration for the NPs (Figures 3C, 3D,
576 4C, and 4D). As shown in Figure 3C, when the concentration for RIF was reduced to 0.5
577 µg/ml (half of MIC), along with 11 µg/ml of ZnONPs, this led to no observable viable growth
578 of H37Rv *Mtb*. Similarly, INH at a concentration of 0.05 ug/ml (half of MIC) completely
579 blocked viability of mycobacterial cells in presence of lower dose of ZnONPs (11 µg/ml)
580 (Figure 3D). In another approach, when RIF and INH were added at their respective MIC (1
581 µg/ml and 0.1 µg/ml respectively), in presence of MIC of ZnONPs (5 µg/ml), no viable cells
582 were observed (Figures 3C, 3D). Similarly, in the case of MDR cells, when LFX and MXF
583 were added at their MIC (0.125 and 0.0625 µg/ml respectively)[84,85], a reduction for ZnONPs

MIC occurred from 14 ug/ml to 0.5 ug/ml, with no growth observed at 11 µg/ml (Figures 4C, 4D).

This strategy demonstrates the potential to achieve significant inhibition of H37Rv as well MDR *Mtb* cells at markedly lower concentrations of conventional anti-TB drugs, with the potential to mitigate the cytotoxic effects associated with prolonged drug administration. The observed synergy between lower doses of existing drugs and ZnONPs presents a promising avenue for enhancing the efficacy of TB management while minimizing potential adverse effects.

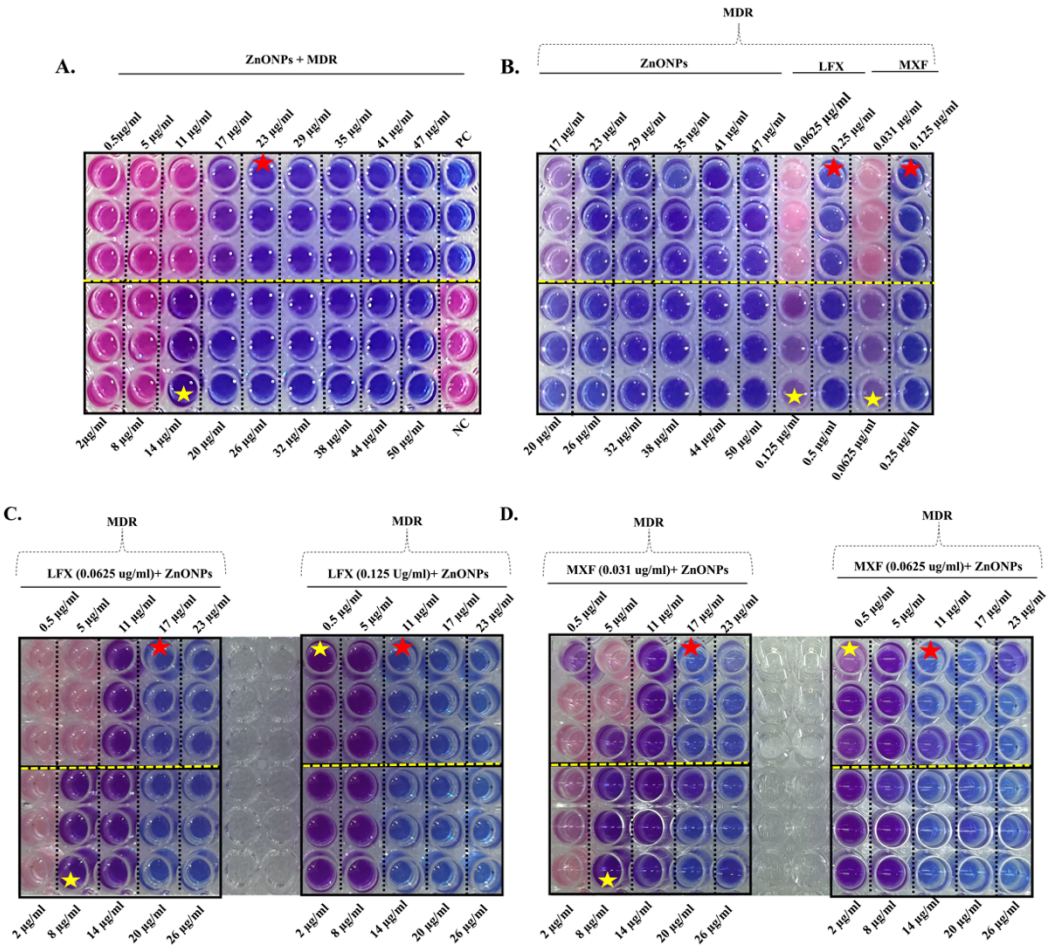


**Figure 4. Alamar blue assay to determine the MIC of ZnONPs towards MDR *Mtb* cells. (A)** Mycobacterial cells were incubated in a 96 well plate, in presence of varied concentrations (0.5 to 50 µg/ml) ZnONPs for 14 days, followed by addition of Alamar Blue reagent. Further incubation at 37ºC for 24 hours, led to colour change in the wells. MIC of ZnONPs was identified as 14 µg/ml where

610 transition of blue to purple colour occurred suggesting partial loss of cell viability among the cells. In
611 contrast, persistence of a blue colour due to complete loss of viable cell population was seen at 23 µg/ml
612 of ZnONPs. Pink cells refer to healthy viable cells resisting inhibitory effect of ZnONPs. **(B)**
613 Comparison of the activity of anti-TB drugs; Levofloxacin (LFX) & Moxifloxacin (MXF) and varied
614 concentration of ZnONPs. All the cells were rendered non-viable (blue) at a concentration of 23 µg/ml
615 for the ZnONPs and in presence of LFX (0.25 µg/ml), MXF (0.125 µg/ml) and at higher concentration.
616 The MIC for LFX & MXF as shown in this study coincided with the known values of 0.125 and 0.0625
617 µg/ml respectively [84,85]. Synergistic activity of ZnONPs and anti-TB drugs; **(C)** LFX & **(D)** MXF. $10^6$
618 CFU of bacterial cells were grown in presence of varied concentrations of ZnONPs and the drugs. A
619 combination of LFX (0.0625 µg/ml) + ZnONPs (17 µg/ml) & LFX (0.125 µg/ml) + ZnONPs (11 µg/ml)
620 successfully yielded non-viable cells (blue). Likewise, MXF (0.031 µg/ml) + ZnONPs (17 µg/ml) &
621 MXF (0.0625 µg/ml) + ZnONPs (11 µg/ml) combinations resulted in non-proliferating cells (blue). Red
622 stars- complete loss of viability & Yellow stars- partial loss of viable cells (purple) at a lower
623 concentration of NPs. MDR: Multidrug-resistant, LFX: Levofloxacin, MXF: Moxifloxacin.
624

625 *3.4 ZnONPs exhibit bactericidal effects on drug-sensitive and MDR Mtb* cells

626 Current work validated the interaction between ZnONPs and *Mtb* SufB, which influenced cell
627 viability, and this can be attributed to the production of a non-functional SufB protein via
628 splicing inhibition, a vital component for *Mtb* survival [11,13]. The observed decrease in viability
629 could also be associated with a cumulative effect of mycobacterial membrane damage activity
630 induced by ZnONPs [40]. To substantiate this hypothesis, we performed a scanning electron
631 microscopy (SEM) analysis, employing various ZnONPs concentrations; a lower concentration
632 of 0.5 µg/ml, two effective concentrations of 17 and 23 µg/ml (MBC for ZnONPs towards
633 H37Rv and MDR *Mtb* cells), and 50 µg/ml, the upper limit for toxicity. These concentrations
634 were selected to cover the effective range of ZnONPs for *in vitro* splicing studies, and MBC
635 values identified by Alamar blue assay & spread plate method.

636 Treatment with ZnONPs at a concentration of 0.5 µg/ml induced minor alterations in the
637 bacterial morphology. However, exposure to concentrations of 17 µg/ml, 23 µg/ml, and 50
638 µg/ml led to extensive membrane disruption, cell-fusion, and cytoplasmic leakage

accompanied by a complete loss of cellular morphology (Figures 5A and 5B). Thus, SEM analysis offers substantial evidence of the membrane-damaging activity of ZnONPs towards H37Rv and MDR *Mtb* isolates. This uniform activity of ZnONPs against both drug-sensitive and MDR *Mtb* cells validates our previous observations on antimycobacterial effectiveness detected via Alamar blue assay. This result is particularly significant in the context of MDR-TB, where conventional antibiotic treatments encounter substantial obstacles.

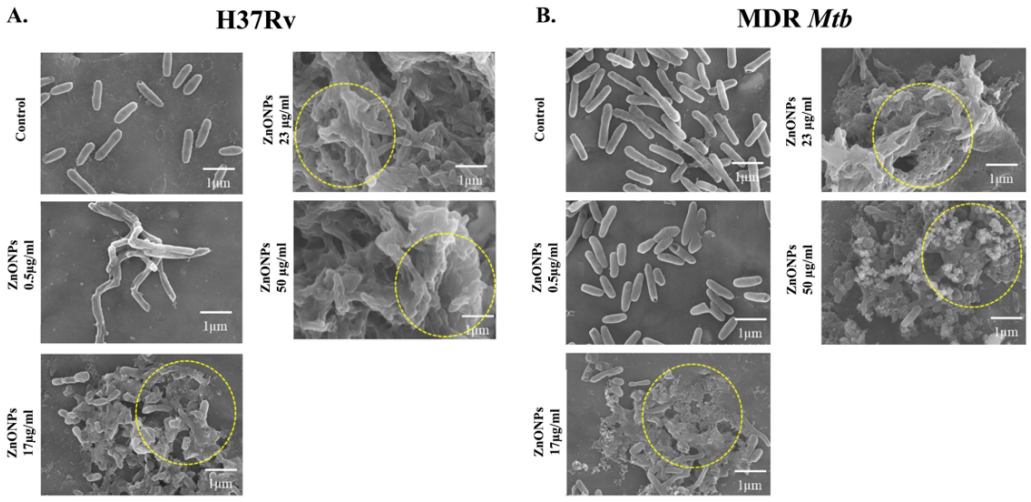


**Figure 5. SEM analysis displaying bactericidal role of ZnONPs on *Mycobacterium tuberculosis (Mtb)*** cells **(A)** H37Rv **(B)** MDR *Mtb* isolates. Control (untreated) mycobacterial cells were uniform looking, without any changes in the cell morphology or any evidence of membrane damage. Mild alterations in cellular morphology were noted for both H37Rv, and MDR *Mtb* cells in presence of 0.5 µg/ml of ZnONPs. Dose dependent increase in the severity of cell membrane damage, cell fusion, loss of cellular architecture, were identified among the **(A)** H37Rv and **(B)** MDR *Mtb* isolates, across rest of the ZnONPs test concentration range (17 µg/ml, 23 µg/ml , and 50 µg/ml) (outlined by yellow circles). MDR: Multidrug-resistant *Mtb*

*3.5 ZnONPs rescue Mtb induced changes in infected mice model*

So far, *in vitro* data from this work suggested potent mycobactericidal activity of ZnONPs against H37Rv and MDR *Mtb* isolates, possibly by inhibiting the splicing of essential protein

676 *Mtb* SufB, leading to loss of viability and membrane damage. To further assess this activity in
677 *in vivo* setting, we conducted experiments in mice model.
678 The utilization of *Mtb* H37Ra (H37Rv attenuated strain)-infected mice serves as an established
679 *in vivo* model to evaluate TB infection [87]. Both H37Ra and H37Rv *Mtb* strains are inhibited
680 by similar concentrations of anti-TB drugs as suggested by an earlier work [88]. Hence, the
681 efficacy of ZnONPs-drug combination and recovery from the infection was further tested in
682 H37Ra-infected mice.
683 BALB/6 mice were infected with *Mtb* H37Ra; 1×PBS (placebo), ZnONPs, and drug (RIF)
684 administration commenced four days post-infection and continued for a total of seven days,
685 with mice sacrificed on day 18 post-infection for subsequent histopathological and bacterial
686 burden analysis (experimental design elucidated in Figure 6A). Administration of RIF dosages
687 is based on earlier works published elsewhere [89–91]. Our findings revealed a strong anti-*Mtb*
688 effect of ZnONPs, as evidenced by the analysis of the gross morphology of spleen,
689 histopathological analysis and bacterial burden assay.
690 A significant splenomegaly was observed in the infected mouse which had received 1×PBS as
691 a placebo following infection with H37Ra strain [92–96]. Resistance to this morphological effect
692 was observed in infected mice, receiving RIF (15 mg/kg) alone, ZnONPs (26 and 50 µg/ml),
693 RIF (10 mg/kg) + ZnONPs (26 µg/ml), and RIF (10 mg/kg) + ZnONPs (50 µg/ml). The
694 splenomegaly following H37Ra infection in the aforementioned experimental groups was
695 rescued significantly when ZnONPs was given as a solo treatment at concentration of 26 µg/ml,
696 and 50 µg/ml. Further, the efficacy of RIF at 15 mg/kg was similar to a combination containing
697 a reduced dosage of RIF at 10 mg/kg along with ZnONPs (26 µg/ml, and 50 µg/ml), where a
698 complete rescue from splenomegaly was seen; comparable to the normal sized spleen in healthy
699 cage control mouse (Figure 6B). Likewise, a substantial reduction in mycobacterial load in
700 lungs and spleen were observed in similarly treated mice groups, emphasizing the superior anti-

TB activity of the ZnONPs/RIF combination (Figures 6C and 6D). Bacterial loads were equivalently attenuated when RIF was administered solo at 15 mg/kg or in combination (RIF 10 mg/kg + ZnONPs 26 µg/ml or RIF 10 mg/kg + ZnONPs 50 µg/ml) at a lower concentration. This highlights the synergistic activity of these anti-*Mtb* compounds displaying a higher potential to manage mycobacterial infection.

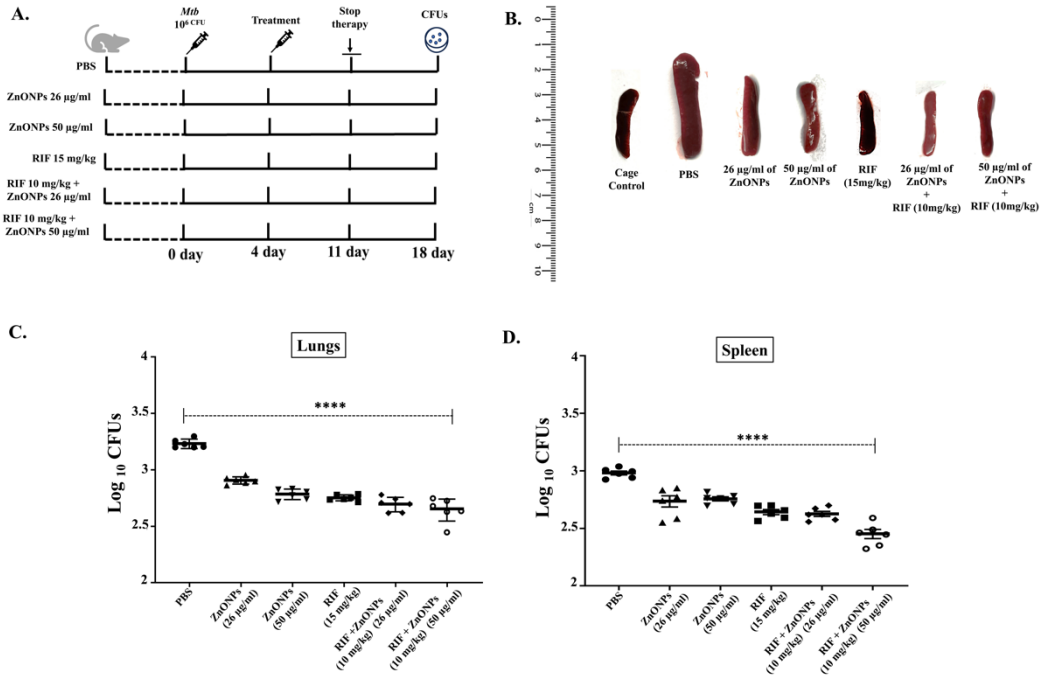


**Figure 6. *In vivo* antimycobacterial effects of ZnONPs in H37Ra infected mice model. (A)** Schematic representation of the experimental design in BALB/c mice (n = 6 in each group). Mice were infected with H37Ra*;* 1×PBS (placebo)*,* NPs and drug administration commenced four days post-infection and continued for a total of seven days, with mice sacrificed on day 18$^{th}$ post-infection. **(B)** Significant splenomegaly was noticed in the infected mouse which had received 1×PBS only. This was not observed in the infected mice, who were given RIF (15 mg/kg) alone, and combinations of RIF (10 mg/kg) + ZnONPs (26 µg/ml), and RIF (10 mg/kg) + ZnONPs (50 µg/ml), where the spleen size was comparable to the normal sized spleen in healthy cage control mouse. The splenomegaly was partially rescued in mice who had received ZnONPs (26 or 50 µg/ml) alone. Bacterial burden in the **(C)** lungs, and **(D)** spleen of the infected mice was determined by plating the organ lysate on the 7H10 plates after treatment with ZnONPs or 1×PBS for 7 days. Significant reduction in mycobacterial loads was observed in mice groups treated with a combination of RIF (10 mg/kg) + ZnONPs (26 µg/ml), and RIF (10 mg/kg) + ZnONPs (50 µg/ml), emphasizing the superior anti-TB activity of the ZnONPs- RIF

731 combination as compared to RIF alone. Data are presented as mean ± 1 SD (p>0.0001) from values
732 obtained from (n=6) mice.
733

734 Next, histopathological examination of infected lungs and spleen tissues provided additional
735 evidence for the anti-mycobacterial efficacy of ZnONPs. Lungs sections from cage control
736 healthy mice displayed clear lung fields without any evidence of inflammation [Figure 7A(a)].
737 Infected mice group administered with 1×PBS displayed distinct pathological changes in the
738 lungs with noticeable inflammatory infiltrates, indicative of infection induced immune
739 response [Figure 7A(b)] [97]. When administered individually, ZnONPs (26 µg/ml), ZnONPs (50
740 µg/ml), and RIF (15 mg/kg) caused a partial reduction in inflammatory cells within the lungs
741 [Figures 7A(c), (d), and (e)]. On the contrary, mice treated with a combination of ZnONPs (26
742 µg/ml) + RIF (10 mg/kg) and ZnONPs (50 µg/ml) + RIF (10 mg/kg) respectively,
743 demonstrated no inflammatory infiltrations, suggesting their superior anti-mycobacterial
744 action ([Figures 7A(f), and (g)].
745 Similarly, inflammatory changes were noted within the white pulp of the infected splenic
746 tissue, which is a critical component of the organ's immune function [98]. Healthy mice from the
747 cage control group exhibited normal spleen histology with clear differentiation into white and
748 red pulps [Figure 7B(a)] [99] whereas, infected mice treated with 1×PBS, depicted rich
749 inflammatory infiltrates obscuring normal spleen histology [Figure 7B(b)] [100]. A partial
750 reduction in inflammation was observed, along with a restoration of the white and red pulp
751 structures in the spleen of the mice treated with ZnONPs (26 µg/ml), and ZnONPs (50 µg/ml),
752 respectively [Figures 7B(c), and (d)]. Notably, in the mice group that received RIF (15 mg/kg)
753 alone or combination therapy [ZnONPs (26 µg/ml) + RIF (10 mg/kg) and ZnONPs (50 µg/ml)
754 + RIF (10 mg/kg)], there were no inflammatory infiltrations, and distinct white and red pulp
755 structures were evident ([Figures 7B(e), (f), and (g)]. Hence, the efficacy of the combinatorial

approach with a reduced dose of RIF (10 mg/kg) was similar to RIF solo therapy at a higher concentration (15 mg/kg).

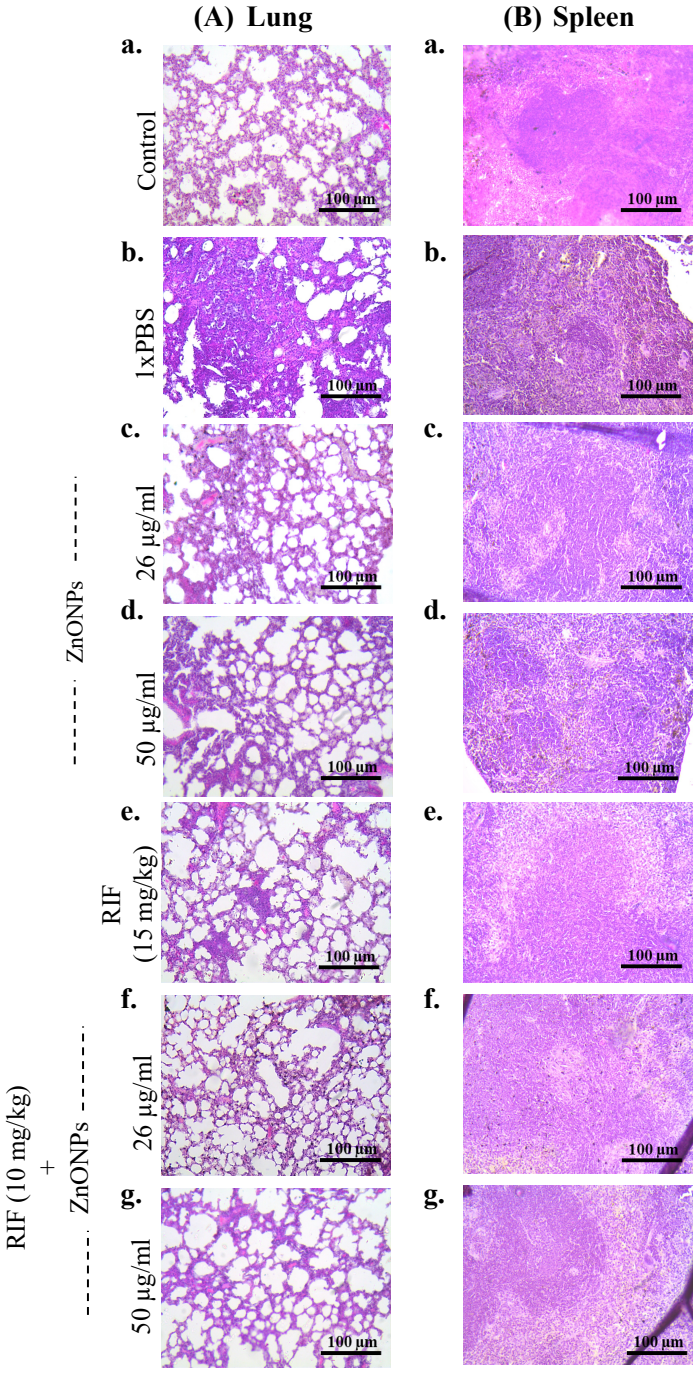


**Figure 7. Histopathology of lungs and spleen from H37Ra infected mice (H37Rv attenuated strain), comparing the efficacy of ZnONPs, RIF, and ZnONPs-RIF combinations. (A)** Lungs sections are stained by H&E staining and processed for visualization by microscopy. **(a)** Histology of

783 uninfected lungs in healthy control mice. **(b-e)** represent tissue sections from infected mice who have
784 received different solo treatments, **(b)** 1×PBS exhibiting prominent aggregates of inflammatory cells;
785 **(c)** 26 ug/ml of ZnONPs, **(d)** 50 ug/ml of ZnONPs , and **(e)** RIF 15 mg/kg displaying partial reduction
786 in immune cells infiltrates; **(f)** RIF (10 mg/kg) + ZnONPs (26 ug/ml), and **(g)** RIF (10 mg/kg) + ZnONPs
787 (50 ug/ml) represent no inflammatory changes and restoration of normal lungs histology. **(B)** Tissue
788 sections from spleen are stained by H&E staining and processed for visualization by microscopy. **(a)**
789 Histology of spleen in uninfected healthy control mice showing well differentiated white and red pulp
790 structures. **(b-e)** represent tissue sections from infected mice who have received different solo
791 treatments; **(b)** 1×PBS exhibiting heavy immune cell aggregates obliterating white and red pulps; **(c)**
792 26 ug/ml of ZnONPs, **(d)** 50 ug/ml of ZnONPs, are displaying partial rescue from inflammatory
793 infiltrates; **(e)** RIF 15 mg/kg**, (f)** RIF (10 mg/kg) + ZnONPs (26 ug/ml), and **(g)** RIF (10 mg/kg) +
794 ZnONPs (50 ug/ml)**,** either of these treatments when given to infected mice, restored normal spleen
795 histology with no evidence of inflammation. Images represent different experimental groups of mice
796 visualized under 10X magnification. H&E- Hematoxylin and eosin staining; RIF- Rifampicin
797

798 These observations support a potential therapeutic effect of the ZnONPs against
799 *Mycobacterium tuberculosis* (*Mtb*). A concurrent mode of action combining, SufB splicing
800 inhibition by ZnONPs along with inhibition of bacterial RNA polymerase due to RIF, and
801 ZnONPs mediated membrane damage, possibly facilitates complete resolution of inflammation
802 restoring normal spleen and lung histology [101]. Taken together, these findings provide a strong
803 foundation for further investigation into the mechanisms underlying the *in vivo* anti-
804 mycobacterial activity of ZnONPs towards drug-sensitive as well as MDR TB. Additionally,
805 long-term studies evaluating the safety and sustained efficacy of ZnONPs will be crucial for
806 assessing their potential as a viable therapeutic option.

807 **4. Conclusion**

808 One of the major milestones of the United Nations Sustainable Development Goals (SDGs) is
809 to end TB by 2030 [102]. Besides aiming for accessible patient care with attenuated
810 hospitalization rate, WHO also calls for "adoption to innovations" in TB management [2]. The
811 escalating challenge of drug-resistant TB, necessitates the exploration of novel therapeutic
812 strategies such as nanomedicine. Current work investigates into the mycobactericidal role of

813 the ZnONPs against both H37Rv *Mtb* strain and MDR *Mtb* isolates, by blocking generation of
814 crucial SufB protein via intein splicing inhibition .
815
816
817
818
819
820
821

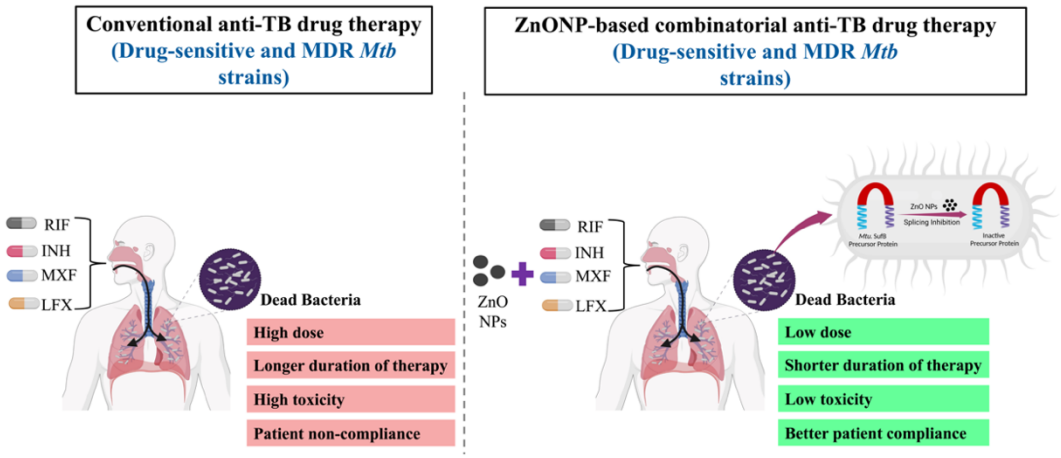


822
823
824 **Figure 8. Schematic diagram illustrating the proposed mechanism for higher efficacy of**
825 **combination therapy in managing drug-susceptible and MDR TB, contrasting with**
826 **conventional drug therapy.** ZnONPs and RIF/INH or MXF/LFX combination exhibits superior
827 therapeutic potential possibly via a dual approach: targeting the mycobacterial viability by splicing
828 regulation to inhibit generation of essential protein SufB, further supported by the potent
829 antimycobacterial action of anti-TB drugs. Multidrug-resistant (MDR), Rifampicin (RIF), Isoniazid
830 (INH), Moxifloxacin (MXF), Levofloxacin (LFX).
831
832 A series of *in vitro* experiments, encompassing Bradford assays, UV-Visible spectroscopy,
833 DLS, zeta potential, and Transmission Electron Microscopy (TEM), have collectively
834 substantiated the interaction between the ZnONPs and the SufB protein. The Alamar Blue
835 assay and Scanning Electron Microscopy (SEM) analysis further elucidated the bactericidal
836 effects of the ZnONPs on H37Rv and MDR *Mtb* cells, which was correlated to the inhibitory
837 effects of the ZnONPs on splicing and cleavage reactions of SufB precursor protein. Thus
838 ZnONPs and the SufB protein interaction induced a significant alteration in the *Mtb* viability
839 possibly due to loss of protein's biological activity. While SEM confirmed extensive
840 mycobacterial membrane damage, the Alamar blue assay highlighted the superior efficacy of

841 a combination therapy (ZnONPs-INH/RIF & ZnONPs-LFX/MXF), where the effective dosage
842 of the anti-TB drugs were reduced by half towards both drug-sensitive strain and MDR *Mtb*
843 isolates [82–85]. Next, *in vivo* experiments in infected mice model, validated substantial anti-
844 mycobacterial activity of ZnONPs-RIF combination against the *Mtb* H37Ra strain.
845 In the current study, histopathological examination of infected lungs and spleen tissues **(**H&E
846 staining) has provided evidence for the anti-inflammatory efficacy of ZnONPs (Figure 7).
847 These results provided insight into the extent of inflammation and immune cell recruitment,
848 which are the key indicators of the host immune response during *Mtb* infection and
849 management [103-105]. When administered individually, ZnONPs (26 µg/ml), ZnONPs (50
850 µg/ml), and RIF (15 mg/kg) caused a partial reduction in inflammatory cells within the infected
851 lungs & spleen. On the contrary, mice treated with a combination of ZnONPs (26 µg/ml) + RIF
852 (10 mg/kg) and ZnONPs (50 µg/ml) + RIF (10 mg/kg), demonstrated no inflammatory cell
853 infiltrations, suggesting their superior anti-inflammatory action (Figure 7). The observed
854 reduction in inflammatory cells in the ZnONPs + RIF treated mice group suggests a favourable
855 anti-inflammatory and anti-mycobacterial effect [106,107].
856 These collective findings underscore the potential of ZnONPs as a promising additive along
857 with existing anti-TB drugs in the fight against tuberculosis. Herein, we propose a dual mode
858 of action for this ZnONPs-based combinatorial approach: ZnONPs can significantly influence
859 mycobacterial viability by complete blockage of splicing and cleavage reactions to inhibit
860 generation of essential protein SufB, further supported by the potent antimycobacterial action
861 of anti-TB drugs (Figure 8). Since eukaryotes such as humans lack intein sequences, and
862 microbial intein sequences resist mutations, targeted drug development strategy aiming
863 splicing regulation of critical proteins have been proposed as novel mechanisms to manage
864 drug-resistant infections [108]. Current study also highlights the reduction in the effective dosage
865 for the anti-TB drugs in combination with ZnONPs, that will address caveats such as drug

toxicity. However, further research and clinical trials will be essential to validate the safety and efficacy of ZnONPs as a potential supportive treatment option for the infected patients.

This study's uniqueness lies in its innovative approach that demonstrated bactericidal efficacy against both drug-sensitive and MDR *Mtb* isolates, as a significant improvement over earlier research. Furthermore, the inhibition of SufB splicing by ZnONPs provides a new mechanism for managing TB, distinct from existing treatments. Additionally, the reduced dose of RIF/INH and MXF/LFX when combined with ZnONPs may lead to fewer adverse effects and improved patient compliance, especially addressing concerns during extended treatment periods (as in case of disseminated TB). Moreover, the potential toxicity of ZnONPs can be further eliminated by obtaining NPs via green synthesis routes [109,110]. Howbeit, future research should focus on clinical trials to validate these findings and explore the long-term benefits and safety of this combinatorial approach. Current study addresses the growing issue of drug-resistant TB by exploring a new therapeutic approach that can have a significant contribution to the field of TB research and management. Higher efficacy along with lower drug dosage and probable shorter treatment duration may have a positive impact on the overall health cost, facilitating global effort to fight against TB.

**Author contributions**

Deepak Kumar Ojha: Conceptualization, Resources, Data curation, Formal Analysis, Validation, Visualization, Methodology, Writing—original draft, Writing—review & editing; Ashwaria Mehra: Resources, Data curation, Funding acquisition, Validation, Methodology, Writing—review & editing; Sunil Swick Rout: Resources, Data curation, Software, Validation, Visualization; Sidhartha Giri: Resources, Validation, review & editing; Sasmita Nayak: Conceptualization, Resources, Data curation, Formal Analysis, Supervision, Funding acquisition, Validation, Investigation, Visualization, Methodology, Writing—original draft, Project administration, Writing—review & editing.

## Conflicts of interest

There are no conflicts to declare

## Data Availability

The data underlying the present article are available in the article and in its online Supplementary Information.


## Acknowledgements

The plasmids used in the present study are borrowed from Prof. Marlene Belfort's Lab, SUNY, Albany, NY, U.S.A. Our sincere gratitude to the Central Instrumentation facility (CIF) at OUAT (Odisha University of Agriculture & Technology), Bhubaneswar and Dr. S.K Dash for his help in conducting SEM analysis at OUAT Bhubaneswar. We thank to Dr. Sravan Kumar for his help in conducting TEM analysis at the Central Institute of Petrochemicals Engineering and Technology (CIPET), Bhubaneswar. We extend our gratitude to Dr. Sidhartha Giri for providing access to the Biosafety Level 3 (BSL3) laboratory facility at ICMR-RMRC, Bhubaneswar, for smooth conductance of mycobacterial experiments.


## Ethics Statement

The animal study was reviewed and approved/recommended by the IAEC of Kalinga Institute of Industrial technology Deemed to be University (KIIT-DU), Bhubaneswar, Odisha. (Approval No. KSBT/IAEC/2023/2/14.2)


## Funding

This work is supported by Indian Council of Medical Research (ICMR), India (ICMR Project ID: IIRP-2023-7834/F1). A.M. is supported by INSPIRE fellowship (DST/INSPIRE/03/2021/002800/IF 190921); INSPIRE Division, DST, Government of India.

914 **Abbreviations**

915 Ab, antibody; ANOVA, Analysis of Variance; CC , C-terminal cleavage product; IB , inclusion
916 bodies; IPTG, isopropyl β-d-1-thiogalactopyranoside; I, intein; CC, C-terminal cleavage; P,
917 precursor; LE, ligated extein; MDR, multidrug resistant; DS, Drug sensitive ; DR, Dug
918 resistance; *Mtb*, *Mycobacterium tuberculosis*; NC, N-terminal cleavage product; NE, N-extein;
919 Ni-NTA, nickel-nitrilotriacetic acid; PAGE, polyacrylamide gel electrophoresis; PVDF,
920 polyvinylidene fluoride; SI, splicing inactive; SDS, sodium dodecyl sulfate; SEM, Scanning
921 Electron Microscope; SUF, Mobilization of Sulphur; TB, Tuberculosis; TCEP.HCl, tris 2-
922 carboxyl ethyl phosphine. Hydrochloric acid; TNB, 2-nitro-5-thiobenzoic acid; UV–Vis, UV–
923 visible spectroscopy; WT, wild-type; NP, Nanoparticle; ZnO, zinc oxide; H&E; Hematoxylin
924 and eosin.

925 **References**

926


927 1 D. R. Silva, F. C. de Queiroz Mello and G. B. Migliori, *Jornal Brasileiro de Pneumologia*, 2020,
928 **46**, e20200027.

929 2 Geneva: World Health Organization. Global tuberculosis report 2023., Global tuberculosis
930 report 2023, https://www.who.int/teams/global-tuberculosis-programme/tb-reports/global-
931 tuberculosis-report-2023, (accessed 2 July 2024).

932 3 K. J. Seung, S. Keshavjee and M. L. Rich, *Cold Spring Harb Perspect Med*,
933 DOI:10.1101/cshperspect.a017863.

934 4 A. Prasanna and V. Niranjan, *Bioinformation*, 2019, **15**, 261–268.

935 5 S. N. Goossens, S. L. Sampson and A. Van Rie, *Clin Microbiol Rev*, DOI:10.1128/CMR.00141-
936 20.

937 6 K. H. Alzahabi, O. Usmani, T. K. Georgiou, M. P. Ryan, B. D. Robertson, T. D. Tetley and A.
938 E. Porter, 2021, preprint, DOI: 10.1042/ETLS20190154.

939 7 S. Panda, A. Nanda, N. Sahu, D. K. Ojha, B. Pradhan, A. Rai, A. R. Suryawanshi, N. Banavali
940 and S. Nayak, *Biosci Rep*, DOI:10.1042/BSR20212207.

941 8 S. Panda, A. Nanda, S. S. Nasker, A. Mehra, D. K. Ojha, P. S. Mohanty and S. Nayak, *Clin Sci*,
942 DOI:10.1042/CS20230307.

943 9 O. Novikova, P. Jayachandran, D. S. Kelley, Z. Morton, S. Merwin, N. I. Topilina and M.
944 Belfort, *Mol Biol Evol*, DOI:10.1093/molbev/msv271.

10 F. Wayne Outten, 2015, preprint, DOI: 10.1016/j.bbamcr.2014.11.001.

11 G. Huet, M. Daffé and I. Saves, *J Bacteriol*, 2005, **187**, 6137–6146.

12 H. K. Chahal, Y. Dai, A. Saini, C. Ayala-Castro and F. W. Outten, *Biochemistry*, DOI:10.1021/bi901518y.

13 G. Huet, J. P. Castaing, D. Fournier, M. Daffé and I. Saves, *J Bacteriol*, 2006, **188**, 3412–3414.

14 K. W. Jayawardana, H. S. N. Jayawardena, S. A. Wijesundera, T. De Zoysa, M. Sundhoro and M. Yan, *Chemical Communications*, DOI:10.1039/c5cc04251h.

15 P. V Mohanan, V. G. Reshma, S. Syama, S. Sruthi, S. C. Reshma and N. S. Remya, *Curr Drug Metab*, DOI:10.2174/1389200218666170925122201.

16 M. Vallet-Regí, B. González and I. Izquierdo-Barba, 2019, preprint, DOI: 10.3390/ijms20153806.

17 A. C. Anselmo and S. Mitragotri, *Bioeng Transl Med*, DOI:10.1002/btm2.10003.

18 G. T. Tietjen and W. M. Saltzman, *Sci Transl Med*, DOI:10.1126/scitranslmed.aad6645.

19 A. Gallud, H. Líbalová and B. Fadeel, *Nanomedicine*, DOI:10.2217/nnm.15.79.

20 T. Sun, Y. S. Zhang, B. Pang, D. C. Hyun, M. Yang and Y. Xia, 2014, preprint, DOI: 10.1002/anie.201403036.

21 J. N. BARRY and A. A. VERTEGEL, *Nano Life*, DOI:10.1142/s1793984413430010.

22 S. J. Park, 2020, preprint, DOI: 10.2147/IJN.S254808.

23 S. R. Saptarshi, A. Duschl and A. L. Lopata, *J Nanobiotechnology*, DOI:10.1186/1477-3155-11-26.

24 D. Peer, J. M. Karp, S. Hong, O. C. Farokhzad, R. Margalit and R. Langer, 2007, preprint, DOI: 10.1038/nnano.2007.387.

25 K. K. Jain, 2005, preprint, DOI: 10.1016/j.cccn.2005.03.014.

26 Y. Barenholz, 2012, preprint, DOI: 10.1016/j.jconrel.2012.03.020.

27 X. Hou, T. Zaks, R. Langer and Y. Dong, 2021, preprint, DOI: 10.1038/s41578-021-00358-0.

28 J. Theron, J. A. Walker and T. E. Cloete, 2008, preprint, DOI: 10.1080/10408410701710442.

29 A. Gogos, K. Knauer and T. D. Bucheli, *J Agric Food Chem*, DOI:10.1021/jf302154y.

30 J. Mou, Z. Liu, J. Liu, J. Lu, W. Zhu and D. Pei, *Drug Deliv*, DOI:10.1080/10717544.2019.1571121.

31 C. Pushpalatha, J. Suresh, V. S. Gayathri, S. V. Sowmya, D. Augustine, A. Alamoudi, B. Zidane, N. H. Mohammad Albar and S. Patil, *Front. Bioeng. Biotechnol*, 2022, DOI: 10.3389/fbioe.2022.917990.

32 X. Li, C. Yuan, Q. Chen, Q. Xue, J. Mou and P. Wang, *Med Oral Patol Oral Cir Bucal*, 2023, **28**, e487–e495.

33 Y. Wang, H. Hua, W. Li, R. Wang, X. Jiang and M. Zhu, *J Dent*, 2019, **80**, 23–29.

34 C. Petchthanasombat, T. Tiensing and P. Sunintaboon, *J Colloid Interface Sci*, 2012, **369**, 52–57.

35 E. M. El-Diasty, M. A. Ahmed, N. Okasha, S. F. Mansour, S. I. El-Dek, H. M. A. El-Khalek and M. H. Youssif, *Rom J Biophys*, 2013, **23**, 191–202.

36 S. Raha and M. Ahmaruzzaman, *Nanoscale Adv*, 2022, **4**, 1868-1925, DOI: 10.1039/d1na00880c.

37 S. Jha, R. Rani and S. Singh, 2023, preprint, DOI: 10.1007/s10904-023-02550-x.

38 M. Heidary, S. Z. Bostanabad, S. M. Amini, A. Jafari, M. G. Nobar, A. Ghodousi, M. Kamalzadeh and D. Darban-Sarokhalil, *Infect Drug Resist*, DOI:10.2147/IDR.S221408.

39 W. Lin, S. Fan, K. Liao, Y. Huang, Y. Cong, J. Zhang, H. Jin, Y. Zhao, Y. Ruan, H. Lu, F. Yang, C. Wu, D. Zhao, Z. Fu, B. Zheng, J. F. Xu and J. Pi, *Front Cell Infect Microbiol*, DOI:10.3389/fcimb.2022.1074533.

40 A. J. Caron, I. J. Ali, M. J. Delgado, D. Johnson, J. M. Reeks, Y. M. Strzhemechny and S. M. McGillivray, *Front Microbiol*, 2024, **15**, 1394078.

41 S. V. Gudkov, D. E. Burmistrov, D. A. Serov, M. B. Rebezov, A. A. Semenova and A. B. Lisitsyn, 2021, preprint, DOI: 10.3389/fphy.2021.641481.

42 P. Sun, S. Ye, S. Ferrandon, T. C. Evans, M. Q. Xu and Z. Rao, *J Mol Biol*, DOI:10.1016/j.jmb.2005.09.039.

43 B. W. Poland, M. Q. Xu and F. A. Quiocho, *Journal of Biological Chemistry*, DOI:10.1074/jbc.275.22.16408.

44 L. Zhang, Y. Zheng, Z. Xi, Z. Luo, X. Xu, C. Wang and Y. Liu, *Mol Biosyst*, DOI:10.1039/b903144h.

45 P. Van Roey, B. Pereira, Z. Li, K. Hiraga, M. Belfort and V. Derbyshire, *J Mol Biol*, DOI:10.1016/j.jmb.2006.12.050.

46 S. Panda, A. Nanda, S. S. Nasker, D. Sen, A. Mehra and S. Nayak, 2021, preprint, DOI: 10.1016/j.biochi.2021.03.006.

47 D. Woods, S. Vangaveti, I. Egbanum, A. M. Sweeney, Z. Li, V. Bacot-Davis, D. S. Lesassier, M. Stanger, G. E. Hardison, H. Li, M. Belfort and C. W. Lennon, *mBio*, DOI:10.1128/mBio.01403-20.

48 R. Afarin, F. Ahmadpour, M. Hatami, S. Monjezi and S. Igder, *Heliyon*, 2024, **10**, e31925.

49 Q. Lin, Y. Jing, C. Yan, X. Chen, Q. Zhang, X. Lin, Y. Xu and B. Chen, *Int J Nanomedicine*, 2024, **Volume 19**, 5381–5395.

50 B. Naiel, M. Fawzy, A. E. D. Mahmoud and M. W. A. Halmy, *Sci Rep*, 2024, **14**, 13459.

51 A. Nanda, S. S. Nasker, A. K. Kushwaha, D. K. Ojha, A. K. Dearden, S. K. Nayak and S. Nayak, *Front Bioeng Biotechnol*, DOI:10.3389/fbioe.2021.773303.

52 E. Suhartono, I. Thalib, I. Aflanie, Z. Noor and R. Idroes, in *IOP Conference Series: Materials Science and Engineering*, 2018, vol. 350.

53 P. K. Grzyska, R. P. Hausinger and D. A. Proshlyakov, *Anal Biochem*, 2010, **399**, 64–71.

54 J. Saikia, M. Yazdimamaghani, S. P. Hadipour Moghaddam and H. Ghandehari, *ACS Appl Mater Interfaces*, DOI:10.1021/acsami.6b09950.

55 G. Su, H. Jiang, B. Xu, Y. Yu and X. Chen, *Mol Pharm*, DOI:10.1021/acs.molpharmaceut.8b00612.

56 A. M. Clemments, C. Muniesa, C. C. Landry and P. Botella, *RSC Adv*, 2014, **4**, 29134–29138.

57 A. Nanda, S. S. Nasker, A. K. Kushwaha, D. K. Ojha, A. K. Dearden, S. K. Nayak and S. Nayak, *Front Bioeng Biotechnol*, 2021, **9**, 773303.

58 A. Sasidharan, J. E. Riviere and N. A. Monteiro-Riviere, *J Mater Chem B*, 2015, **3**, 2075–2082.

59 K. Friedel, M. A. Popp, J. C. J. Matern, E. M. Gazdag, I. V. Thiel, G. Volkmann, W. Blankenfeldt and H. D. Mootz, *Chem Sci*, DOI:10.1039/C8SC01074A.

60 L. Zhang, Y. Zheng, B. Callahan, M. Belfort and Y. Liu, *Journal of Biological Chemistry*, DOI:10.1074/jbc.M110.171124.

61 K. V. Mills, B. M. Lew, S. Q. Jiang and H. Paulus, *Proc Natl Acad Sci U S A*, DOI:10.1073/pnas.95.7.3543.

62 K. V. Mills and H. Paulus, *Journal of Biological Chemistry*, DOI:10.1074/jbc.M011149200.

63 J. P. Gangopadhyay, S. qin Jiang and H. Paulus, *Anal Chem*, DOI:10.1021/ac020756b.

64 H. Chan, C. S. Pearson, C. M. Green, Z. Li, J. Zhang, G. Belfort, A. Shekhtman, H. Li and M. Belfort, *Journal of Biological Chemistry*, DOI:10.1074/jbc.M116.747824.

65 K. Punjabi, S. Mehta, R. Chavan, V. Chitalia, D. Deogharkar and S. Deshpande, *Front Microbiol*, DOI:10.3389/fmicb.2018.02207.

66 W. Zhou, B. Yang, Y. Zou, K. Rahman, X. Cao, Y. Lei, R. Lai, Z. F. Fu, X. Chen and G. Cao, *Front Microbiol*, DOI:10.3389/fmicb.2021.658637.

67 E. M. Longhin, N. El Yamani, E. Rundén-Pran and M. Dusinska, *Frontiers in Toxicology*, DOI:10.3389/ftox.2022.981701.

68 C. Mahendra, M. N. Chandra, M. Murali, M. R. Abhilash, S. B. Singh, S. Satish and M. S. Sudarshana, *Process Biochemistry*, DOI:10.1016/j.procbio.2019.10.020.

69 S. Sharma, E. Gelman, C. Narayan, D. Bhattacharjee, V. Achar, V. Humnabadkar, V. Balasubramanian, V. Ramachandran, N. Dhar and N. Dinesh, *Antimicrob Agents Chemother*, DOI:10.1128/AAC.03205-14.

70 S. Panda, T. K. Rout, A. D. Prusty, P. M. Ajayan and S. Nayak, *Advanced Materials*, DOI:10.1002/adma.201702149.

71 L. Abarca-Cabrera, P. Fraga-García and S. Berensmeier, 2021, preprint, DOI: 10.1186/s40824-021-00212-y.

72 C. Eisner, H. Ow, T. Yang, Z. Jia, E. Dimitriadis, L. Li, K. Wang, J. Briggs, M. Levine, J. Schnermann and M. G. Espey, *J Appl Physiol*, DOI:10.1152/japplphysiol.01068.2011.

73 G. Yan, Y. Huang, Q. Bu, L. Lv, P. Deng, J. Zhou, Y. Wang, Y. Yang, Q. Liu, X. Cen and Y. Zhao, *J Environ Sci Health A Tox Hazard Subst Environ Eng*, DOI:10.1080/10934529.2012.650576.

74 A. M. Florea, F. Splettstoesser and D. Büsselberg, *Toxicol Appl Pharmacol*, DOI:10.1016/j.taap.2007.01.022.

75 R. V.G. and M. P.V., *Colloids Surf B Biointerfaces*, DOI:10.1016/j.colsurfb.2017.05.069.

76 M. Kokkinopoulou, J. Simon, K. Landfester, V. Mailänder and I. Lieberwirth, *Nanoscale*, DOI:10.1039/c7nr02977b.

77 E. L. Han, S. Tang, D. Kim, A. M. Murray, K. L. Swingle, A. G. Hamilton, K. Mrksich, M. S. Padilla, R. Palanki, J. J. Li and M. J. Mitchell, *Nano Lett*, DOI:10.1021/ACS.NANOLETT.4C05186/SUPPL_FILE/NL4C05186_SI_001.PDF.

78 B. Baral, B. Panigrahi, A. Kar, K. D. Tulsiyan, U. Suryakant, D. Mandal and U. Subudhi, *Mol Ther Nucleic Acids*, 2023, **33**, 493–510.

79 G. Huet, M. Daffé and I. Saves, *J Bacteriol*, DOI:10.1128/JB.187.17.6137-6146.2005.

80 V. Valdiglesias, A. Alba-González, N. Fernández-Bertólez, A. Touzani, L. Ramos-Pan, A. T. Reis, J. Moreda-Piñeiro, J. Yáñez, B. Laffon and M. Folgueira, *Int J Mol Sci*, DOI:10.3390/ijms241512297.

81 B. N. Patil and T. C. Taranath, *Int J Mycobacteriol*, DOI:10.1016/j.ijmyco.2016.03.004.

82 S. S. Hakkimane, V. P. Shenoy, S. L. Gaonkar, I. Bairy and B. R. Guru, *Int J Nanomedicine*, 2018, **13**, 4303–4318.

83 M. Getahun, H. M. Blumberg, G. Ameni, D. Beyene and R. R. Kempker, *PLoS One*, 2022, **17**, e0274426.

84 H. Zheng, W. He, W. Jiao, H. Xia, L. Sun, S. Wang, J. Xiao, X. Ou, Y. Zhao and A. Shen, *BMC Infect Dis*, 2021, **21**, 1–6.

85 Q. Sun, K. Cheng, X. Liao, W. Zhao, C. Wang, C. Wang, J. Yan, L. Dong, F. Wang, G. Jiang, H. Huang, Z. Guo and G. Wang, *J Med Microbiol*, 2024, **73**, 001825.

86 F. B. Perler, *Nucleic Acids Res*, DOI:10.1093/nar/30.1.383.

87 N. Kumari, R. Sharma, J. Ali, G. Chandra, S. Singh and M. Y. Krishnan, *Tuberculosis*, DOI:10.1016/j.tube.2024.102479.

88 M. T. Heinrichs, R. J. May, F. Heider, T. Reimers, S. K. B. Sy, C. A. Peloquin and H. Derendorf, *Int J Mycobacteriol*, DOI:10.4103/ijmy.ijmy_33_18.

89 J. E. M. De Steenwinkel, R. E. Aarnoutse, G. J. De Knegt, M. T. Ten Kate, M. Teulen, H. A. Verbrugh, M. J. Boeree, D. Van Soolingen and I. A. J. M. Bakker-Woudenberg, *Am J Respir Crit Care Med*, DOI:10.1164/rccm.201207-1210OC.

90 I. M. Rosenthal, R. Tasneen, C. A. Peloquin, M. Zhang, D. Almeida, K. E. Mdluli, P. C. Karakousis, J. H. Grosset and E. L. Nuermberger, *Antimicrob Agents Chemother*, DOI:10.1128/AAC.00912-12.

91 H. M. Blumberg, W. J. Burman, R. E. Chaisson, C. L. Daley, S. C. Etkind, L. N. Friedman, P. Fujiwara, M. Grzemska, P. C. Hopewell, M. D. Iseman, R. M. Jasmer, V. Koppaka, R. I. Menzies, R. J. O'Brien, R. R. Reves, L. B. Reichman, P. M. Simone, J. R. Starke and A. A. Vernon, *Am J Respir Crit Care Med*, 2003, **167**, 603–662.

92 B. Pottakkat, A. Kumar, A. Rastogi, N. Krishnani, V. K. Kapoor and R. Saxena, *Gut Liver*, DOI:10.5009/gnl.2010.4.1.94.

93 D. A. Lestari, N. Rahadiani and R. A. Syaiful, *Int J Surg Case Rep*, DOI:10.1016/j.ijscr.2021.105966.

94 Y. Tojo, S. Yanagisawa, E. Miyauchi and M. Ichinose, 2018, preprint, DOI: 10.1016/j.ijid.2017.12.009.

95 L. Kremer, J. Estaquier, I. Wolowczuk, F. Biet, J. C. Ameisen and C. Locht, *Infect Immun*, DOI:10.1128/IAI.68.7.4264-4273.2000.

96 A. Masumi, K. Mochida, K. Takizawa, T. Mizukami, M. Kuramitsu, M. Tsuruhara, S. Mori, K. Shibayama, K. Yamaguchi and I. Hamaguchi, *Inflamm Regen*, DOI:10.1186/s41232-016-0024-3.

97 A. Nava, A. C. Hahn, T. H. Wu and T. F. Byrd, *Front Immunol*, DOI:10.3389/fimmu.2022.1017540.

98 S. M. Lewis, A. Williams and S. C. Eisenbarth, 2019, preprint, DOI: 10.1126/sciimmunol.aau6085.

99 B. S. Steiniger, *Immunology*, DOI:10.1111/imm.12469.

100 S. M. Szczepanek, J. T. McNamara, E. R. Secor, P. Natarajan, L. A. Guernsey, L. A. Miller, E. Ballesteros, E. Jellison, R. S. Thrall and B. Andemariam, *American Journal of Pathology*, DOI:10.1016/j.ajpath.2012.07.034.

101 W. Wehrli, *Rev Infect Dis*, DOI:10.1093/clinids/5.Supplement_3.S407.

102 United Nations, The Sustainable Development Goals Report 2023, https://unstats.un.org/sdgs/report/2023/, (accessed 2 July 2024).

103 B. Jee, Central European Journal of Immunology, 2020, 45, 99–103, DOI:10.5114/ceji.2020.94711.

104 F. Rahman, Front Immunol, 2024, 15, 143790, DOI:10.3389/fimmu.2025.1560113.

105 B. Singh, I. Pahuja, P. Yadav, A. Shaji, S. Chaturvedi, A. Ranganathan, V. P. Dwivedi and G. Das, J Infect Dis, 2024, 229, 1509–1518, DOI: 10.1093/infdis/jiad460.

106 F. E. A. Hayford, R. C. Dolman, R. Blaauw, A. Nienaber, C. M. Smuts, L. Malan and C. Ricci, Respir Res, 2020, 21, 1–14, DOI: 10.1186/s12931-020-01488-9.

107 V. M. Kroesen, M. I. Gröschel, N. Martinson, A. Zumla, M. Maeurer, T. S. van der Werf and C. Vilaplana, Front Immunol, 2017, 8, 280326, DOI: 10.3389/fimmu.2017.00772.

108 H. Paulus, *Frontiers in Bioscience-Landmark*, 2003, **8**, 1157–1165.

109 R. Álvarez-Chimal and J. Ángel Arenas-Alatorre, in *Green Chemistry for Environmental Sustainability - Prevention-Assurance-Sustainability (P-A-S) Approach*, 2023.

110 J. Iqbal, B. A. Abbasi, T. Yaseen, S. A. Zahra, A. Shahbaz, S. A. Shah, S. Uddin, X. Ma, B. Raouf, S. Kanwal, W. Amin, T. Mahmood, H. A. El-Serehy and P. Ahmad, *Sci Rep*, DOI:10.1038/s41598-021-99839-z.